29

Extraterrestrial arid surface processes

Gordon L. Wells and James R. Zimbelman

Introduction

The development of arid zone geomorphology has progressed over the past century from ground-level observations of a limited number of locations through the field traverse mapping of sizeable arid areas to a broad-scale overview of global desert regions assisted by aerial photography and satellite imagery. Extraterrestrial investigations of planetary surfaces and landforms have proceeded in exactly the opposite manner. Telescopic observations first provided global overviews of distant planets. The early spacecraft missions of the 1960s relayed hemispheric and regional views, while later missions returned more detailed images comparable to satellite images of the Earth. To date, detailed views seen from the surfaces of other terrestrial planets are restricted to two locations on Mars and four landing sites on Venus. As a result, the approach and scope of our inquiry into arid processes are necessarily different when studying extraterrestrial surfaces. In this review, we attempt to build a picture of the arid surface of Mars starting with a discussion of possible microscale and mesoscale processes and later examining the creation of individual arid landforms and terrains. We conclude with an overview of recent discoveries regarding the surface of Venus and attempt to forecast the course of future planetary missions of interest to arid zone scientists.

Spacecraft exploration of Mars began with three Mariner flyby missions during the 1960s. The initial impression was of a surface much like that of the Moon. This judgement changed following the Mariner 9 mission in 1971–72, which relayed more detailed images showing a surface with many landforms common to Earth. Beginning in the summer of 1976, views from the surface were transmitted by two landing craft. On 20 July 1976, Viking 1 landed on the vast volcanic plain of Chryse Planitia (22.5°N, 47.8°W). Several weeks later, Viking 2 touched down upon Utopia Planitia (48.0°N, 225.6°W), another northern hemisphere plain. During the time of Viking lander data collection, two Viking orbiters imaged the surface from an altitude of about 1500 km.

Though Mars is a small planet, its land-surface area is nearly equal to that of the Earth. Another close similarity is daylength. Because the Martian day is slightly longer than Earth's, events at the Viking landing sites were measured in *Sols*, or Martian solar days, following each landing. Mars also has distinct seasons, but due to the eccentricity of its orbit, the seasons are of unequal length. The

Arid Zone Geomorphology: Process, Form and Change in Drylands, 2nd edition. Edited by David S. G. Thomas.

Table 29.1 *Physical characteristics of Earth, Mars and Venus*

	Earth	Mars	Venus
Planetary mass (kg)	5.98×10^{24}	6.44×10^{23}	4.87×10^{24}
Planetary radius (km)	6369	3394	6052
Land surface area (km^2)	1.47×10^{6}	1.45×0^{6}	4.61×10^{6}
Acceleration due to gravity ($m\ s^{-1}$)	9.81	3.72	8.85
Composition of atmosphere	N_2 (0.78) O_2 (0.21) H_2O (<0.03) A (0.01)	CO_2 (0.95) N_2 (0.027) A (0.016)	CO_2 (0.97) N_2 (0.03) $SO_2 + S_2$ (<0.001)
Mean surface pressure (mb)	1016	7.5	~90 000
Surface temperature (°C)	−53–57	−128–−28	374–465
Rotation period (hours and minutes)	23 h 56 m	24 h 37 m	5832 h (retrograde)
Revolution period (yr)	1.000	1.881	0.615
Orbit eccentricity	0.017 Range: 0.01–0.05	0.093 Range: 0.009–0.14	0.007
Obliquity* (degrees)	23.5 Range: 21.8–24.4	25.2 Range: ~12–38 (0.2–51.4)*	~179

Source: Hartmann (1972); Leovy (1979); Carr (1981).
*Obliquity history values calculated by Bills (1990).

convention for reference to Martian seasons is the aerocentric longitude (L_s), where in the northern hemisphere the vernal equinox occurs at $L_s = 0°$, summer solstice at $L_s = 90°$, autumnal equinox at $L_s = 180°$ and winter solstice at $L_s = 270°$.

The basic physical characteristics of Earth, Mars and Venus (Table 29.1) permit a wide range of surface environments. One of the major goals in the development of geomorphological theory is the creation of explanations for landscape processes based upon general principles and not merely the results of descriptive speculation. The surfaces of Mars and Venus offer laboratories for testing the assumptions of terrestrial theories under conditions where such variables as gravity, atmospheric pressure and surface temperature are different.

Rock disintegration processes on Mars

The primordial mechanism for rock disintegration on planetary surfaces was brecciation caused by impacting meteorites. Following the first several hundred million years of solar system history, a decline in the rate of meteorite impacts reduced the quantity of newly fragmented materials. On Earth, Mars and Venus, the availability of volatiles allowed the chemical breakdown of impact breccia (regolith), and on Earth the plate tectonic regime produced a chemically differentiated crust suited to chemical alteration by a variety of processes. The chemical weathering processes occurring on Mars are in several ways unlike those on Earth, because the Martian lithosphere does not undergo plate motion, subduction and crustal recycling, and its regolith is composed primarily of mafic to ultramafic basalts.

PRESENCE OF WATER

Attempts to estimate the total amount of outgassed water during Martian history have arrived at figures representing an equivalent global surface layer of liquid water ranging in depth from 100 to 500 m (Carr 1981; 1986; Squyres 1984; Donahue 1995). The entire inventory of observable water in the modern atmosphere and ice caps represents a surface layer less than 10 m in depth (Rossbacher and Judson 1981). Analyses performed on soil samples collected at the Viking landing sites

confirm that at least some of the water has become chemically bound with surficial sediments. The materials at the landing sites show high concentrations of iron (as anticipated from the rusty red surface coloration of the Martian landscape), sulphur, calcium and magnesium (Baird *et al.* 1976). The relative abundances suggest source rocks of mafic composition, probably basalts. The Viking results led Baird *et al.* (1976) to conclude that the fine-grained materials on Mars are predominantly iron-rich clays with additional components of magnesium sulphate (10%), carbonate (5%) and iron oxides (5%). The production of smectite clays on Mars may follow several pathways (Carr 1981), including hydrothermal alteration in the volcanic regions (Griffith and Arvidson 1994), groundwater alteration in subsurface aquifers (Burns and Fisher 1990; Burns 1994) and, perhaps, ultraviolet-catalysed reactions with a monolayer of water coating fine-grained basaltic sediments (Huguenin 1976; Stephens *et al.* 1994).

FROST WEATHERING AND DISAGGREGATION PROCESSES

The frost point of water on Mars is −75°C, and all regions poleward of 40° latitude receive at least some seasonal H_2O frost accumulation usually mixed with CO_2 frost in a clathrate structure. At both Viking landing sites, water vapour was saturated in the atmosphere, and lander measurements appear to confirm a seasonal exchanged between surface materials and the atmosphere (Moore *et al.* 1987; Moore and Jakosky 1989). Laboratory experiments by Huguenin (1982), which simulated the Martian frost cycle, produced chemical weathering of silicates (olivine) as a result of the incorporation of hydrogen ions from the H_2O frost. In addition to chemical weathering, frost may serve mechanically to disaggregate fine-grained surface materials in the high-latitude regions. The precipitation of frost occurs when atmospheric dust particles, which serve as nucleation sites for equatorial water vapour, arrive over the winter hemisphere high latitudes. The dust–H_2O ice particles may also condense CO_2 ice at its frost point of −125°C. In regions near the poles, the dust–H_2O–CO_2 ice particles coat the surface as a seasonal extension of the polar cap. If these condensates occupy pore spaces among the fine surficial sediments and condense additional trace amounts of surface water vapour, frost-wedging may liberate fine particles that would then be available for aeolian transport.

SALT WEATHERING

An unexpected result of the Viking chemical analyses of Martian surface samples was the discovery of a high concentration of sulphate ($MgSO_4$ and $NaSO_4$), carbonate ($CaCO_3$) and chloride (NaCl) salts in the Martian soil. The amount of sulphur was found to be enriched in samples taken from thin layers of duricrust atop aeolian drift deposits and in pebble-sized soil aggregates, when their composition was compared to that of unconsolidated fine materials. The excess sulphur content strongly indicates that salt weathering is an active process on Mars (Clark *et al.* 1976; Clark and Van Hart 1981), and that thin layers of iron-rich clay particles are cemented by sulphate and carbonate minerals (Toulmin *et al.* 1977). Diffusion of salts to the surface by water vapour passing through the substrate could lead to the formation of widespread duricrust layers over periods of 10^5–10^6 years (Jakosky and Christensen 1986) The most dramatic 'geomorphological event' to occur during observations at the Viking 1 landing site was the slope failure and slumping of duricrust material covering a drift deposit near the base of a large boulder (Figure 29.1). The drift deposits in the vicinity of the Viking 1 lander give the appearance of being stripped by deflation. If this interpretation is correct, duricrust formation has proceeded with sufficient rapidity to encase aeolian drift materials as the deposits are in the process of being deflated and removed from the area. In areas of stable or accumulating aeolian deposits, salt weathering may lead to the production of considerably thicker duricrusts.

Salt weathering may attack competent Martian rocks along several possible routes (Malin 1974) even in the absence of liquid water. As occurs in terrestrial environments discussed in Chapter 3, hydration by water vapour of salts trapped in surface rock pores may physically

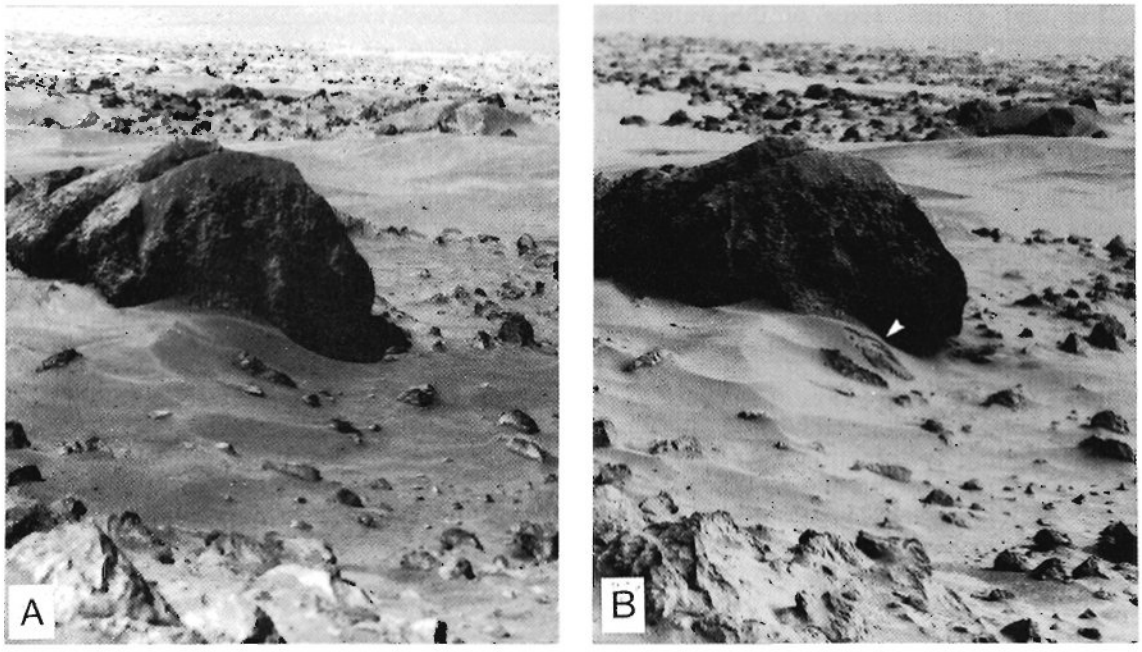

Figure 29.1 *Two views of the Viking 1 landing site taken on (A) VL-1 Sol 25 and (B) Sol 239 record a slump of duricrust material upon a drift deposit. [(A) VL1 #11A143; (B) #11C162]*

destroy rocks, as may the diurnal thermal expansion and contraction of salt crystals trapped inside pore spaces of rocks having a different expansion coefficient.

AEOLIAN ABRASION

Apparently wind-faceted and pitted rocks are plentiful near the Viking landing sites (Figure 29.2), and wind-tunnel experiments (Greeley *et al.* 1984) simulating Martian conditions have confirmed high rates of aeolian abrasion. In fact, the simulated rates are enormous, if basalt or quartz grains are used as impactors. Abrasion rates in the range 0.0003–0.002 cm yr^{-1} have been calculated by Greeley *et al.* (1984) and result from the high initial velocities of Martian particles in saltation and their high terminal velocities under conditions of low atmospheric drag. Paradoxically, the Martian surface near the landing sites is covered with large and probably very ancient rocks (Mutch and Jones 1978; Sharp and Malin 1984), while orbital imagery reveals concentrations of small- to medium-sized craters near the Viking 1 landing site, which indicate a surface age of more than 3 billion years (Arvidson *et al.* 1979). At the simulated rate of aeolian abrasion, all rocky landforms on the scale of 100 m would be abraded to near base-level in less than 50 million years.

At least three factors may explain the discrepancy between the rate of aeolian abrasion modelled by wind-tunnel experiments and the degree of surface modification actually observed. Broad regions of Mars presently serve as sediment sinks for aeolian materials, while other areas show signs of the removal of formerly extensive aeolian mantles. Perhaps in some regions (e.g. around the South Pole) a blanket of aeolian deposits protected the ancient surface from abrasion (Plaut *et al.* 1988). A second possibility follows from the character of saltation on Mars. Both landing sites display rocky surfaces. In the Martian atmosphere, typical saltation path lengths span several metres and require sandy surfaces over such distances for a saltation cloud to develop fully. The distribution of rocks could effectively dampen the saltation flux and reduce the rate of abrasion (Williams and Greeley 1986). Finally,

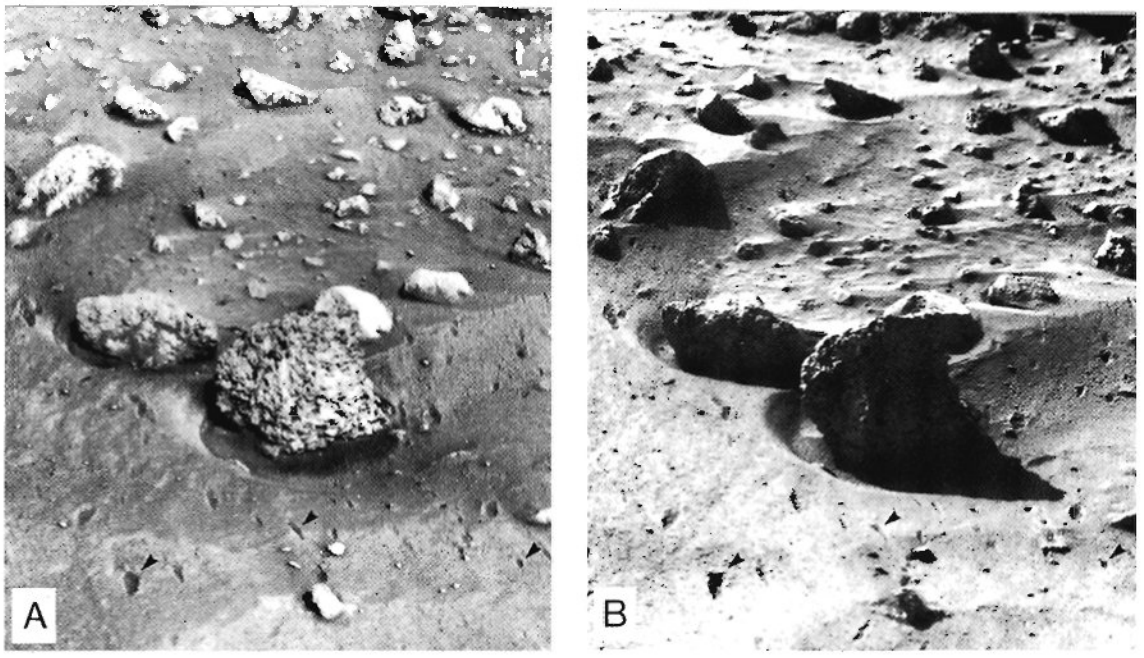

Figure 29.2 *Two views under different illumination conditions show wind-faceted and pitted rocks at the Viking 1 landing site. Arrows point to small impacts penetrating duricrust by clasts dislodged during the firing of the lander descent rocket. [(A) VL1 #11B144; (B) #11A078]*

most saltating particles on Mars probably do not consist of intact mineral grains. Energetic collisions during saltation would lead to short lifetimes for basalt fragments and other 'kamikaze' grains similar to terrestrial quartz sands (Sagan *et al.* 1977). Clay aggregates dislodged from duricrusts provide the most reasonable candidates for saltation (Greeley 1979), and aggregates formed as a sublimation residue of dust-nucleated ice may supply saltable materials in the polar regions (Saunders and Blewett 1987; Thomas and Weitz 1989; Herkenhoff and Murray 1990a). Impact abrasion by these low-density particles would be much less effective than with intact mineral grains.

Transport by suspension, saltation and creep on Mars

As on Earth (see Chapter 16), the primary modes of aeolian transport on Mars are suspension, saltation and creep. However, the boundary conditions governing Martian aeolian processes result in transport events having different magnitudes, frequencies and durations to those of comparable events on Earth (Greeley and Iversen 1985).

DUST DEVILS

During summer months, in the lower boundary layer of the clear, cold, thin Martian atmosphere, the large vertical temperature gradient above the relatively warm surface may support intense free convection. Under these conditions during periods of near calm, thermals will rise into the deep Martian convective layer. Gentle surface winds crossing topographic irregularities may create sufficient basal shear to induce vortices lifting dust into the rising thermal. The resulting dust devils have been observed on high-resolution Viking orbiter images of Arcadia Planitia and Phlegre Montes between 30°N and 45°N (Thomas and Gierasch 1985). Of the 99 dust vortices detected, most dust funnels achieved heights of 1.0–2.5 km. Estimated dust mass suspended aloft in the typical Martian

dust devil is 3000 kg (Thomas and Gierasch 1985).

Although never directly imaged, circumstantial evidence points to the existence of much larger Martian aeolian vortices. Dark linear filaments approximately 0.5 km wide with lengths of 2–75 km lie along approximately parallel tracks on the plains of the southern hemisphere between 30°S and 60°S (Grant and Schultz 1987). The filaments display short gaps and make their appearance seasonally from midsummer until early autumn with slight changes in orientation detected from year to year. These dark filaments may result from surface dust removal and concentration of sand-sized sediments by tornadic vortices sweeping across the southern hemisphere mid-latitudes. Confirmation of such storms occurring in a southern hemisphere 'tornado alley' awaits their detection by future Mars-orbiting spacecraft.

BAROCLINIC AND KATABATIC DUST STORMS

Global weather systems may produce local dust storms whenever the poleward temperature gradient is sufficiently large to generate intense zonal circulation across the mid-latitudes in the form of baroclinic waves. Numerical simulations of Martian general circulation indicate that surface wind velocities in excess of the saltation threshold should accompany the passage of strong baroclinic waves (Mass and Sagan 1976; Pollock *et al.* 1981; Barnes *et al.* 1993; Greeley *et al.* 1993), and examples of dust-transporting extratropical cyclones have been observed in a few instances (Hunt and James 1979; Kahn *et al.* 1992). On the surface, meteorological instruments aboard the Viking landers recorded peak gust velocities of 20–26 $m\,s^{-1}$ during the passage of dust storms (Hess *et al.* 1977; Moore *et al.* 1987).

Most observations of local dust storms document a second type of circulation that operates on a regional scale. These dust storms are produced by katabatic outflow from receding frost outliers of the polar caps and diurnal winds descending areas of high relief (Lee *et al.* 1982; Magalhaes and Gierasch 1982; Kahn *et al.* 1992). The great majority of dust storms take place from late spring until after perihelion passage, $L_s = 250°$, near the time of the southern hemisphere summer solstice (Peterfreund 1985),when the latitudinal temperature gradient close to the retreating frost outlier reaches its most extreme value, as does surface heating near the subsolar point. The frequent occurrence of point-source dust plumes rising from areas recently covered by the seasonal frost cap leads to speculation about the role of frost-wedging in the production of fines for transport by suspension after water ice has sublimed (Figure 29.3). During the modern climatic epoch on Mars, the combination of fine particles released by frost-wedging and strong katabatic surface winds sweeping along the subliming frost cap has created a significant dust source in the southern hemisphere (Christensen 1988). Based upon Viking Infrared Thermal Mapper (IRTM) observations, Viking camera images and terrestrial telescopic sightings, Peterfreund (1985) located 156 dust storm events, 79% of which originated in the southern hemisphere.

MARTIAN GLOBAL DUST STORMS

When the Mariner 9 spacecraft approached Mars in November 1971, the entire surface was obscured by a global dust storm. Such enormous dust storms follow an evolutionary sequence governed by the thermal properties of the Martian atmosphere and global circulation. Of the large dust storms, which have been observed to grow to global proportions, all originated south of the equator near the time of southern hemisphere perihelion, $L_s = 250° \pm 60°$ (Briggs *et al.* 1979; Kahn *et al.* 1992).

Once entrained in the Martian atmosphere, dust absorbs incoming radiation, which is then reradiated as sensible heat. Differential heating of dusty and clear air parcels promotes convective turbulence leading to high-velocity surface winds along the dust storm margin which, in turn, serve to raise additional dust. On a larger scale, regional dust storms form an atmospheric thermal blanket that interacts with clear-air regions of lower heat capacity to produce strong, thermally driven tidal winds (Leovy and Zurek 1979). These winds will be particularly effective in raising dust from areas along the

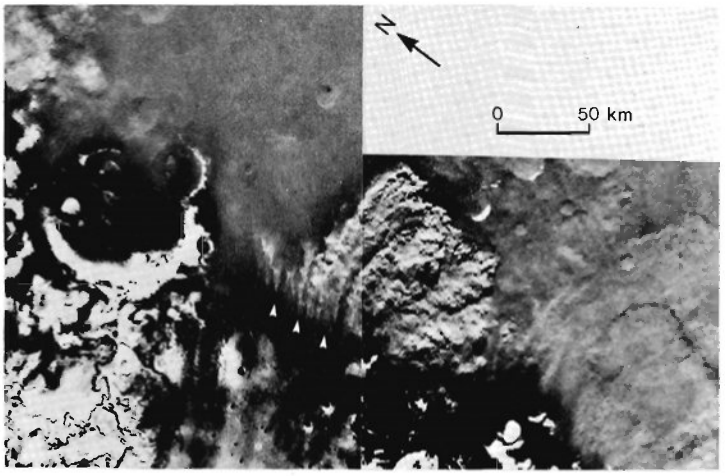

Figure 29.3 *Point-source dust plumes (arrows) rise from an area recently covered by the seasonal H_2O frost cap in the Aonia Terra region (68°S, 69°W) of the Martian southern hemisphere. [VO #248B55, #248B56]*

sunset terminator, where a region of dust warmed by radiative heating adjoins a rapidly cooling region of clear air. A regional dust storm driven by convective turbulence and thermal tides may propagate to achieve global dimensions.

During the late spring and summer, global circulation on Mars is dominated by a cross-equatorial Hadley cell (Haberle *et al.* 1993). The rising limb of the cell is located near the subsolar point in the summer hemisphere, and the descending limb over the winter hemisphere mid-latitudes (Toon *et al.* 1980; Pollock *et al.* 1981; Magalhaes 1987). The presence of a dusty atmosphere in the southern hemisphere near the time of northern winter solstice greatly amplifies the Hadley circulation (Haberle *et al.* 1993). Once pervaded with dust, the global atmosphere becomes stabilised because only the upper portion is effectively heated (Haberle 1986a; 1986b). Convective turbulence is smothered near the surface by an almost isothermal environmental lapse rate. Over a period of several weeks, dust settles out of the atmosphere. The northern polar region, with its condensing frost cap, acts as a primary sediment sink where the dust from global storms serves in the condensation process to nucleate H_2O and CO_2 ice (Toon *et al.* 1980; Barnes 1990).

Global dust storms constitute the primary geomorphological process occurring on Mars during the present climatic epoch. Laboratory measurements show that small amounts of deposited dust (less than $10^{-3}\,g\,cm^{-2}$) can result in reflectance values comparable to optically thick dust layers, even when deposited upon a dark surface (Wells *et al.* 1984). Viking lander cameras at both landing sites recorded the deposition of a thin (less than 1 mm thick), red dust layer following the two global dust storms of 1977 (Guinness *et al.* 1982). The surface brightening was most noticeable in the areas surrounding the Viking 2 landing site on Utopia Planitia (Figure 29.4). As viewed from the Viking orbiters, the northern hemisphere surfaces of Syrtis Major and Acidalia Planitia brightened measurably immediately after the 1977 global storms, then gradually darkened again over the following months (Christensen 1988). By contrast, Hellas Planitia, a southern hemisphere basin and site of frequent dust outbreaks, appears to be a sediment source currently undergoing net erosion by aeolian processes (Moore and Edgett 1993).

BRIGHT AND DARK WIND-STREAKS

Extending from many topographic highpoints, crater rims in particular, are light or dark albedo streaks in the equatorial and mid-latitude portion of Mars between 40°N and 40°S (Figure 29.5). Both types of streak are intimately connected to the occurrence of global dust storms. Bright streaks are interpreted to be deposits of fine material which have been concentrated preferentially in protected

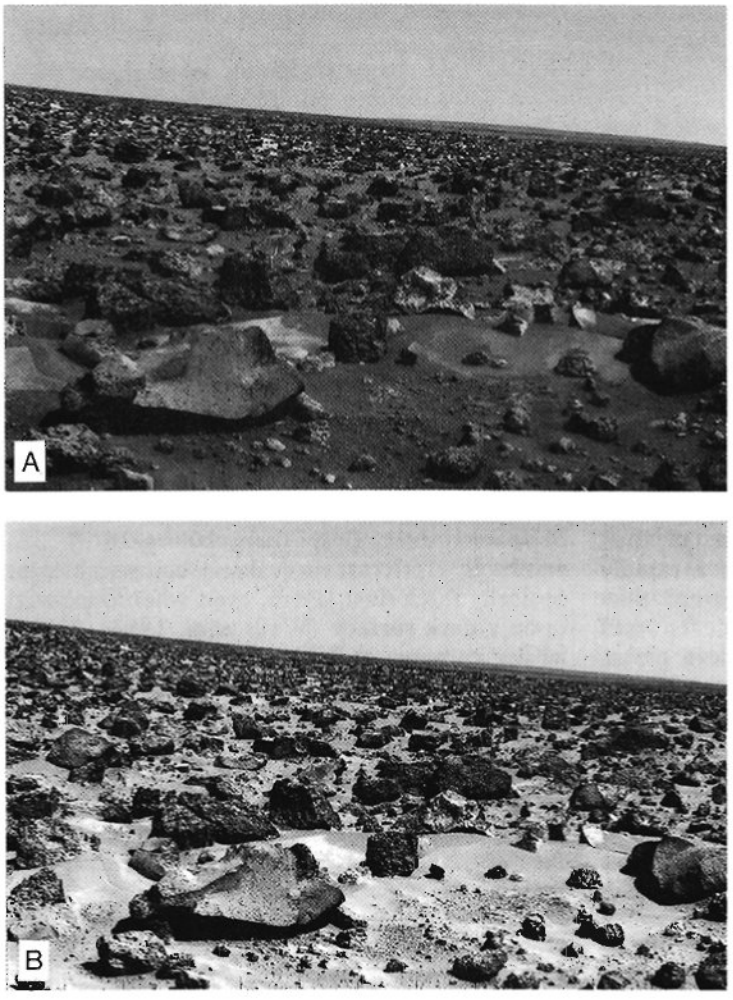

Figure 29.4 *The brightening of the surface around the Viking 2 landing site following dust deposition by the 1977 global storms is apparent in two surface views made under similar illumination conditions on (A) VL-2 Sol 30 prior to the dust storms and (B) after the dustfall. [(A) VL2 #22A252; (B) #22G085]*

wind-shadow zones during dustfalls from global storms (Veverka *et al.* 1981; Greeley *et al.* 1992b). Light-coloured streaks are typically wide, exhibit a feather-like structure downwind and reach lengths of 5–20 km. The dark streaks result from deflation in the lee of topographic obstructions by paired horizontal vortices shed from obstacles that accelerate local airflow (Greeley *et al.* 1974). The dark erosional streaks that expose the underlying surface are narrow, sharply defined and attain lengths of 5–30 km (Greeley and Iversen 1985). Whereas the bright streaks are relatively stable features exhibiting only minor changes over the course of several Martian years, the dark streaks largely vanish after deposition of a thin layer of surface dust from a single global dust storm and begin to reform in the period immediately after the dustfall (Thomas and Veverka 1979).

Local differences in bright and dark wind-streak directions and the creation of bright depositional streaks rather than dark erosional streaks have been attributed to differing meteorological conditions in a hypothesis developed by Veverka *et al.* (1981). When radiative heating of dust promotes static stability during the dustfall stge of a global storm, airflow in the boundary layer becomes more laminar, leading to concentrated dust deposition in long wind-shadow zones in the lee of obstacles. Sediments in bright wind-streaks are deposited at this time. After the atmosphere clears, the effect of flow-blocking by terrain diminishes, and vertical motions again

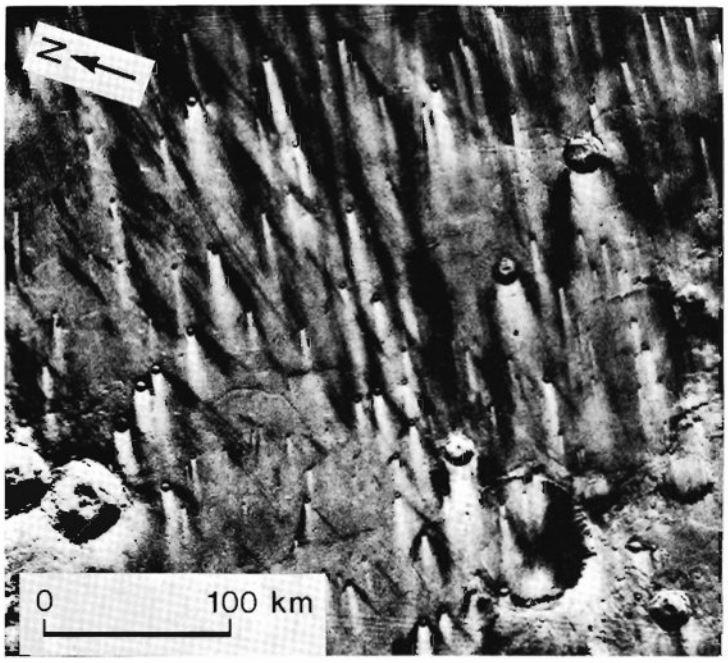

Figure 29.5 *Both bright and dark albedo streaks extend downwind from crater rims in the Syrtis Major region (4°N, 297°W). [VO #496A45]*

predominate in the boundary layer, allowing vortices to scour the recent dustfall layer to create dark wind-streaks.

The global distribution of bright wind-streak directions serves to map the general circulation of Mars at the time of streak formation. Since most bright streaks are formed during global dust storms, the trans-equatorial Hadley circulation of the southern hemisphere late spring and summer is traced by these surface 'weather vanes' (Thomas and Veverka 1979; Lee *et al.* 1982; Greeley *et al.* 1992b; 1993).

MARTIAN AEOLIAN MANTLE

The transport of aeolian sediment across large regions on Mars leads to areas of net sediment accumulation and removal (Thomas 1982; Christensen 1986b; Kahn *et al.* 1992). Regions of relatively high albedo (0.25–0.4) are interpreted to contain more dust than regions of lower albedo (0.1–0.2) (McCord and Westphal 1971; Pleskot and Miner 1981). The subdued surface morphology within regions of higher reflectance is consistent with the presence of a uniformly distributed mantling material (Zimbelman and Kieffer 1979). Our knowledge of the absolute depth of aeolian deposits in an area is limited by the spatial resolution of spacecraft cameras. However, some aspects of the physical properties of Martian surface materials can be inferred from data transmitted by the IRTM sensors on the Viking orbiters.

The equatorial and mid-latitude regions display areas of relatively low thermal inertia interspersed with areas of relatively high thermal inertia (Figure 29.6A). The distribution of particle sizes inferred from thermal inertia values divides Mars into longitudinal sectors (Figure 29.6B). Global circulation patterns influenced by large-scale topography may determine the regional concentrations of fine- and coarse-grained surface materials. It appears significant that the areas of lower thermal inertia are closely correlated with the areas of higher albedo (Kieffer *et al.* 1977).

The absolute thickness of surface materials distributed across the Martian surface can be broadly constrained by remote sensing measurements. In high thermal inertia regions, the fine-particle thickness may be as much as tens of centimetres. Earth-based radar measurements of low thermal inertia areas show a large amount of scattering by surface roughness (Harmon *et al.* 1982). This result suggests an upper limit to the

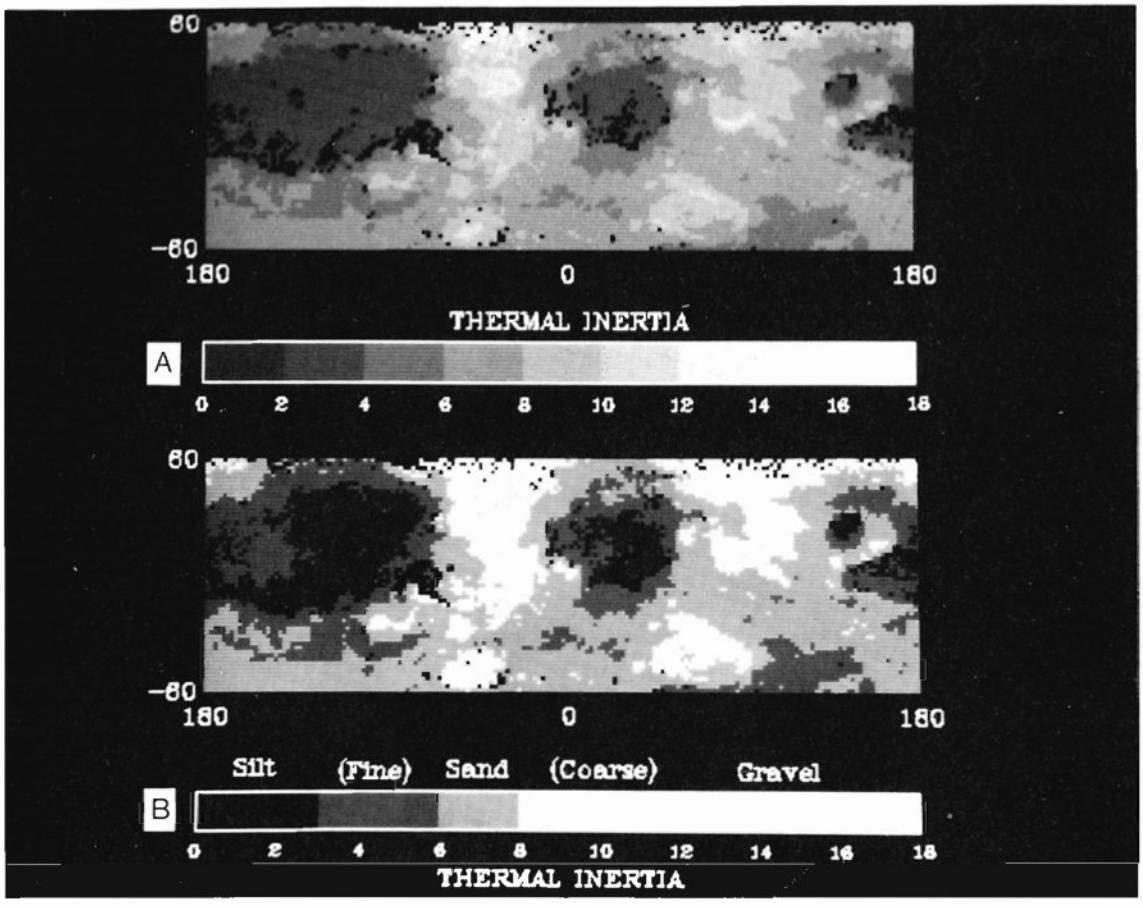

Figure 29.6 *Martian surface thermal inertia in units of* 10^{-3} *cal* $cm^{-3} s^{-1/2} K^{-1}$ *derived from temperatures measured by the Viking IRTM. (A) Data separated by thermal inertia units (0 = lowest; 18 = highest). (B) Data separated according to average particle size for an idealised uniform particle surface (Kieffer* et al. *1973)*

depth of fine materials of 1–2 m (Christensen 1986a; 1986b). Moreover, in low thermal inertia areas, fine materials are not sufficiently thick to mask the thermal effects of more competent materials, such as large blocks or boulders, which are observed in varying abundances over most of the Martian surface (Christensen 1986c). These observations indicate that potentially mobile fine sediments are dispersed around the entire planet.

TRANSPORT BY SALTATION AND CREEP

Experiments performed using the Mars Surface Wind Tunnel (MARSWIT) and Venus Wind Tunnel (VWT) at the NASA Ames Research Center have clarified differences in particle saltation that take place on Earth, Mars and Venus (Figure 29.7). On Mars, the most easily entrained sediment grains have a diameter of 0.115 mm (Iverson and White 1982). Thermal inertia measurements of aeolian sediments held within crater dunefields indicate the presence of considerably coarser grains with diameters of 0.4–0.6 mm (Edgett and Christensen 1991). The lower atmospheric pressure results in threshold friction velocities roughly one order of magnitude higher than terrestrial velocities for lifting particles of similar size. On Mars, a threshold friction speed of 2.4 $m\,s^{-1}$ is required to entrain a 0.1 mm particle with the density of basalt (2.5 $g\,cm^{-3}$). With the arrival of the first

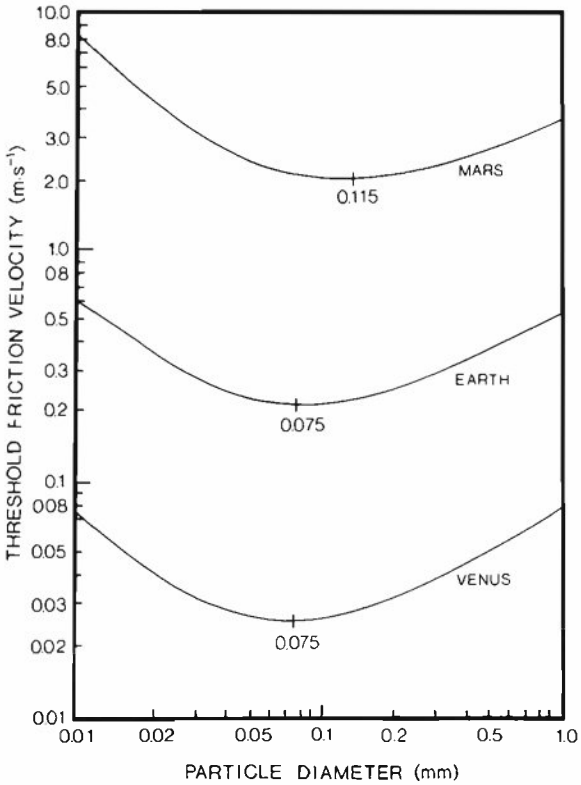

Figure 29.7 *Threshold friction velocities for entraining aeolian sediments on Mars, Earth and Venus as determined by wind-tunnel experiments (modified after Iversen and White 1982)*

global dust storm of 1977, wind velocities measured 1.6 m above the surface at the Viking 1 landing site reached 17.7 $m\,s^{-1}$ with instantaneous gusts of more than 25 $m\,s^{-1}$ (Ryan and Henry 1979). These velocities are close to the required threshold for saltation, when extrapolated to the surface. In a typical terrestrial sand desert, significant saltation may occur during about 10% of the days in a year. Saltation events occur much less frequently on Mars, and probably happen during only 0.01–0.1% of the days in a Martian year. Despite its relative rarity, saltation on Mars should be much more vigorous than on Earth because initial particle velocities are much higher, and atmospheric drag is minimal, leading to high terminal velocities.

Surface creep, or the rolling of grains in traction across the surface, may play a substantially smaller part in aeolian transport on Mars, given the boundary conditions for saltation to be initiated and the anticipated nature of saltation clouds. The very long path lengths of saltating particles cause fewer impacts per unit area under wind conditions just above the saltation threshold. On Mars, surface creep will be inhibited by the relatively small number of neighbouring impacts setting stationary particles rolling across the surface.

Depositional bedforms on Mars

The appearance of Martian dunes, dunefields and ergs suggests a strong connection to bedform sand transport processes in terrestrial deserts. Yet there exist intriguing differences between the two planets in the global distribution of sand dunes and relative abundance of particular dune types.

BARCHANOID AND TRANSVERSE DUNES

Nearly all dunes on Mars are either barchanoid or transverse bedforms (Figure 29.8). Individual barchans appear in planform to be almost identical to their terrestrial counterparts and occur as simple bedforms and as compound megadunes, where smaller, secondary dunes rest atop the major bedform (Breed *et al.* 1979; Tsoar *et al.* 1979). In dunefields, barchans have collided to form barchanoid ridge dunes, and areas with an abundant sediment supply contain transverse ridge dunes. With the exception of isolated dunefields within crater basins (Lancaster and Greeley 1987; Edgett and Christensen 1991), most regions of Martian dunes are situated in the high latitudes between 70°N and 85°N (Ward *et al.* 1985). Whether this asymmetry reflects characteristics of Martian global circulation, latitudinal differences in available sources of sediment or a combination of these factors remains an open question.

A more fundamental question is the composition of Martian dunes. The petrological evolution of Mars has limited the amount of siliceous rock for breakdown into quartz grains, and highly energetic particle collisions over the course of geological time would have long ago smoothed the surface and reduced the saltating population of intact mineral grains to dust-sized

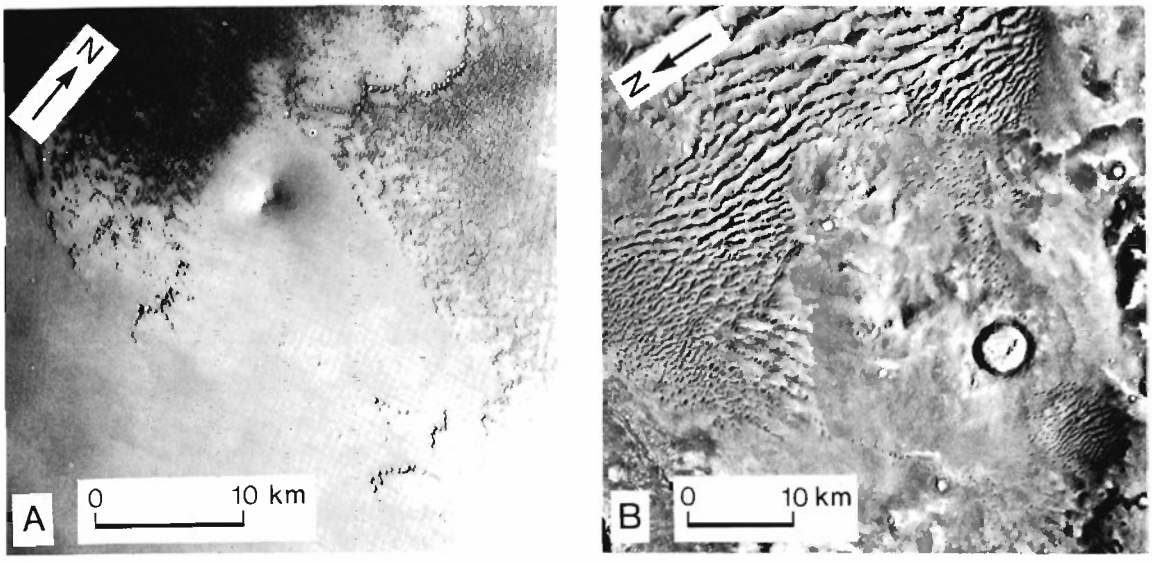

Figure 29.8 *Martian barchan and transverse dunes. (A) Barchans of the North Polar erg (77°N, 97°W). (B) Transverse bedforms in the ancient cratered terrain of the southern hemisphere (47°S, 340°W). [(A) VO #519B27; (B) #575B60]*

fragments. Perhaps the saltating sediments of Mars need not be long-lived to construct bedforms. On Earth, aggregates of clay occasionally are transported to create small dunes with slip faces, even though the entire dune structure becomes cemented after minimal rainfall (Bowler 1973). Dunes composed of silt–clay aggregates are suggested to occur on Mars (Greeley 1979). As a possible terrestrial analogue, the gypsum dunes of White Sands, New Mexico, are barchanoid and transverse bedforms (McKee 1966) constructed by strongly cohering grains. Breed *et al.* (1979) noted close morphological similarities between Martian barchanoid ridges in the northern polar region and those at White Sands in terms of scale width, length and spacing. They also detected groove-like features on Martian dunes comparable to the wind-eroded surfaces of partially cemented gypsum dunes at White Sands.

Many dunes in the northern polar region are covered by frost in the winter. Frost-wedging, chemical weathering and deflation of their surfaces and interdunes may dislodge aggregates from duricrust layers, liberating particles for saltation. So long as Martian saltation events are in equilibrium with aggregate production, the dunes will remain intact. If aggregate production diminishes, the dunes may become etched and grooved by wind erosion.

SCARCITY OF LINEAR DUNES

Unlike terrestrial sand deserts, Mars lacks large concentrations of linear dunes. Painstaking investigation has uncovered only a few examples of linear dunes and other bedforms resulting from bi- and multidirectional sediment-moving winds. The least ambiguous linear bedforms lie within a 70-km-diameter crater in the southern hemisphere (59°S, 343°W), where 4–5 km dune ridges extend from a field of barchanoid dunes (Edgett and Blumberg 1994). In this case, local topographic obstructions appear to influence the direction of winds crossing the crater floor. Limited numbers of Martian star dunes in the Mare Tyrrhenum region are similarly situated in an area subject to local topographic disruptions of regional airflow (Edgett and Blumberg 1994).

Several reasons may explain the scarcity of linear bedforms on Mars. In their discussion of the northern polar region, two investigations (Tsoar *et al.* 1979; Lee and Thomas 1995) point to barchans with elongated wings as

examples of seif dunes. Tsoar *et al.* (1979) suggest that the dunes are in an early stage of bedform evolution. This idea fails to accord with the high degree of bedform organisation displayed by regional megadune patterns, which requires a minimum of several thousand years to develop on Earth and probably much longer on Mars. In an alternative hypothesis, Breed *et al.* (1979) regard the dunes of the northern polar region and other Martian dunefields to be geomorphologically mature formations, where most dunes now lie in topographically restricted areas, such as crater basins. Saltable sediments no longer pass across great distances between sedimentary basins. An analogy can be made to the mass-transport flux of aeolian sediments in the Saharan sand basins (Mainguet and Chemin 1985). In the Sahara, linear dunes are the primary mode of bedform transport from the upwind source regions of a basin and across interbasin sills into topographically confined sediment sinks.

A likely explanation for the scarcity of linear dunes is that Martian saltation events take place under a limited range of meteorological conditions. The climatological setting for these low-frequency events may include only the most energetic phases of Hadley circulation over the equatorial regions, zonal circulation crossing the mid-latitudes, katabatic outflow from the polar caps and downslope winds from high terrain. Each of these systems creates relatively unidirectional airstream trajectories that would lead to the production of barchanoid and transverse bedforms. An atmospheric General Circulation Model of Mars, which incorporates several boundary conditions for surface shear stress reflecting different saltation threshholds, generated theoretical values for the resultant drift potential divided by the total drift potential (RDP/DP ratios) for global regions (Lee and Thomas 1995). The calculated RDP/DP ratios commonly exceed 0.9 and point to unidirectional sediment movement under a unimodal wind regime in most regions of Mars.

ERGS

The North Polar sand sea (Figure 29.9) forms a dark circumpolar collar that reaches its maximum extent between 77–83°N and 110–220°W (Tsoar *et al.* 1979). With an area of approximately 680 000 km^2, the North Polar erg is larger than any individual terrestrial sand sea containing mobile dunes and holds an estimated 1158 km^3 of dune sediment (Lancaster and Greeley 1990).

Two principle circulation patterns are responsible for shaping the dunes of the North Polar erg. Low-pressure fronts tracking along the northernmost latitude of zonal circulation produce dune-forming westerly and southwesterly winds below 80°N. Easterly and northeasterly sand-moving winds have created the dunes above 80°N between 120°W and 240°W in the region nearest to the perennial polar ice cap (Tsoar *et al.* 1979). The airflow regime is the consequence of katabatic winds in the cyclonic circumpolar vortex which follow an outflow pattern traced by frost streaks into dunefields surrounding the perennial ice cap (Howard 1980). The concentration of dark polar dunes into a narrow latitudinal band may be aided by strong surface winds induced along the sharp regional temperature gradient and albedo boundary in a manner similar to the creation of a terrestrial sea breeze (Thomas and Gierasch 1995). The location of dunefields downwind of the polar cap suggests that polar layered deposits are the most likely source of dune sediment (Thomas 1982; Thomas and Weitz 1989; Lancaster and Greeley 1990).

In contrast to Tsoar *et al.* (1979), Breed *et al.* (1979) argued that the North Polar erg is ancient, citing the absence of sand-passing longitudinal dunes, the high degree of organisation in dune patterns and signs of wind erosion upon some dune surfaces. Another feature that signifies an older age for the erg is the occurrence of several very large barchanoid ridges in the upwind areas of dunefields. These 'framing dunes' are now displaced from neighboring dune ridges located downwind by a distance several times the mean wavelength separating other ridges in the dunefields. Such a circumstance can arise only after many reconstitution cycles (the period required for a bedform to move its own length). In an earlier stage of bedform development, more rapidly migrating upwind dunes collided with a barchanoid ridge causing its volume and height to increase and rate of advance to slow. The adjacent

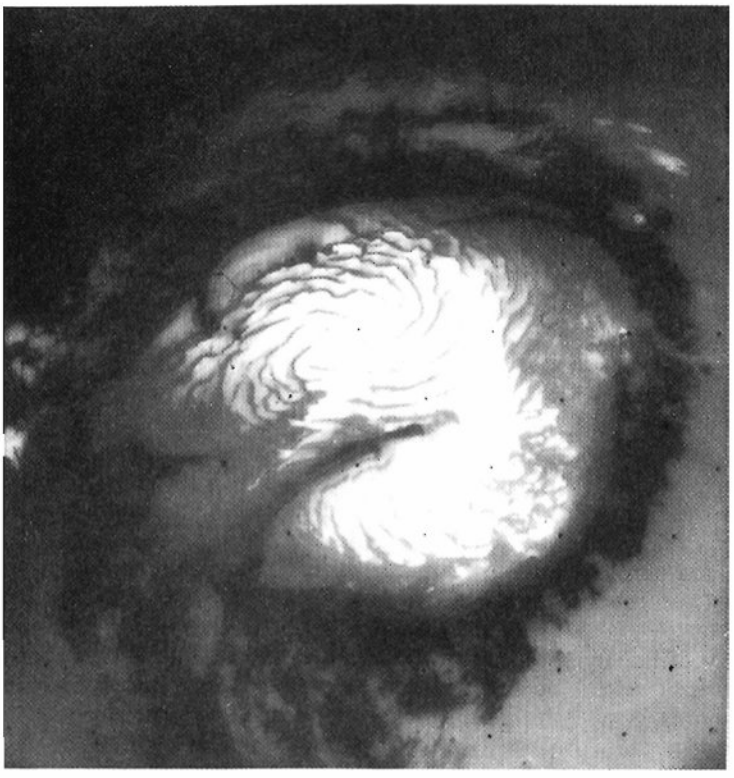

Figure 29.9 *The dark dune collar of the North Polar erg surrounds the perennial H_2O ice cap of the North Pole. [Mariner 9 #4297-46]*

downwind ridges of the dunefield then began to move away from the larger barchanoid ridge. The existence of windward framing dunes separated at some distance from other ridges together with the likelihood that reconstitution cycles for Martian megadunes are considerably longer than the *c.* 1000-year periods for equivalent bedforms on Earth belie the creation of the North Polar erg on the *c.* 10^4–10^6-year timescale of the present climatic period.

Aeolian erosion on Mars

In the vicinity of the Viking landing sites, pitted rocks with wind-faceted forms have been created by aeolian abrasion (Figure 29.2). Though abrasion has modified many smaller rocks at the landing sites, the presence of boulder fields of rather pristine appearance and probable age of more than a billion years demonstrates that, in regions where lag materials protect the surface, wind erosion occurs very slowly. On a broader scale, the stripping of aeolian mantles and other friable deposits in several regions confirms that aeolian erosion proceeds more rapidly where surface units are composed of fine-grained, loosely consolidated materials (Figure 29.10).

AERODYNAMICALLY SCULPTURED LANDFORMS

Yardangs are most plentiful on the equatorial plains overlain by layered deposits. Mature terrestrial yardangs have a width-to-length ratio of about 1:4 (Ward and Greeley 1984). By contrast, in many cases Martian yardangs appear to be extremely elongated, a factor that Ward (1979) ascribes to more intensive abrasion within the corridors separating Martian yardangs than that which occurs on Earth. The paucity of detailed field research and laboratory experiments dealing with the evolution of terrestrial yardangs limits an attempt to understand Martian yardang elongation, but the spacing of joints and fracture patterns within the layered deposits and granulometric characteristics of

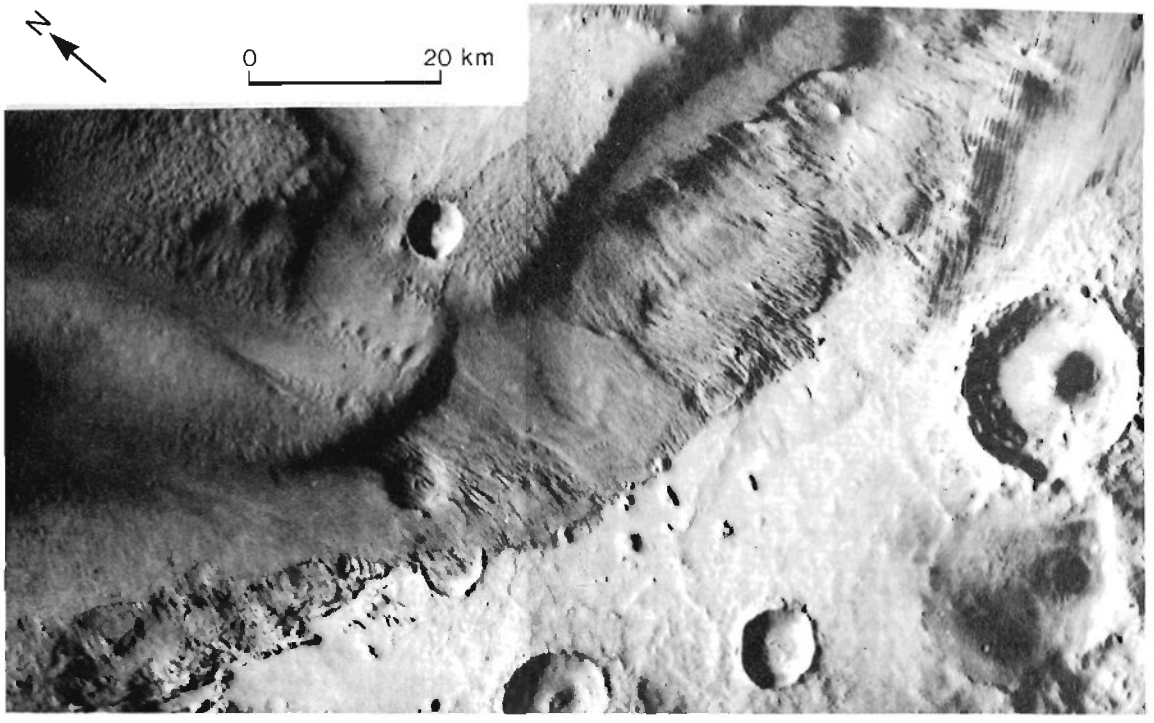

Figure 29.10 *The aeolian stripping of a mantle of layered deposits in the Amazonis Planitia region (11°S, 177°W) exhumes an ancient cratered surface. [VO #438S01, #438S03]*

the sediments may also contribute to the development of elongated yardangs.

Though some yardangs occur in the mid-latitude and polar regions of Mars, the majority are located on the equatorial plains. These low-latitude yardang concentrations resemble terrestrial wind-sculptured landforms developed upon ignimbrite sheets in the central Andes (Figure 29.11). The proximity of the Amazonis Planitia layered deposits to the Olympus Mons and Tharsis Montes volcanic massifs has led some investigators to conclude that the layered deposits were emplaced by pyroclastic flows (Scott and Tanaka 1982; Ward *et al.* 1985). Other features suggest they are layers of an aeolian mantle deposited in a sedimentary basin to the west of Tharsis Montes. For instance, several of the layers are capped by a resistant unit approximately 5–10 m thick. Terrestrial ignimbrites form welded horizons only near the base of flow surges and have easily eroded surfaces. An indurated horizon within the uppermost portion of a layer in the Martian deposits appears out of character with ignimbrite formation, but is in keeping with the anticipated weathering processes of a loess-like aeolian mantle.

DEFLATION BASINS

The most Earth-like type of wind-eroded basin on Mars takes the form of a cusp-shaped depression in which the apex of the cusp points upwind along the axis of deflation (Figure 29.16). The blunted, downwind portion of cuspate basins can be more than 100 m deep, while the apex grades to the level of the surrounding surface. On Earth, shallower basins but with similar shapes in planform have been created upon sandy surfaces along the margins of ancient lake-beds in the western United States, where loosely consolidated sediments favour lateral deflation in the direction of the formative wind (Goudie and Wells 1995).

The most unusual Martian deflation basins are distinctly crescentic pits developed upon the

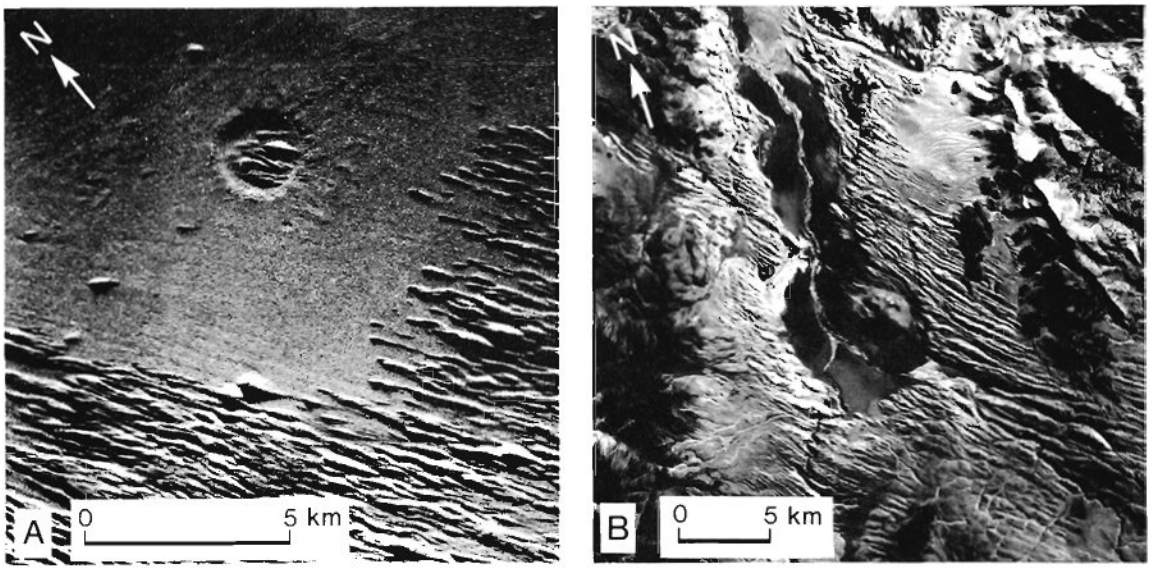

Figure 29.11 *Martian yardangs (A) of the Amazonis Planitia region (1°N, 171°W) closely resemble terrestrial yardangs (B) formed upon the Cerro Galan ignimbrite of northwestern Argentina (25.5°S, 66.8°W). [(A) VO #7728A64; (B) Landsat TM 50787-13503]*

equatorial layered deposits. These small basins have classically aerodynamic shapes similar to an inverted mould cast from a barchan dune. All occur at the windward base of incipient yardangs, where the most intense abrasion occurs upon yardangs formed on Earth (Ward and Greeley 1984). No basins of similar morphology have been reported from investigations of terrestrial yardang localities.

Slope processes on Mars

Gravity serves to modify slopes on all planetary bodies. On most planetary surfaces, this involves the slumping of debris, including the rolling of individual rocks detached from upper slopes by local meteorite impacts or seismic tremors. Martian mass movements extend from the gradual slope retreat and talus creation of dry mass-wasting to the sudden and catastrophic emplacement of giant debris avalanches.

EXPOSURE OF SUBSURFACE VOLATILES

Of all the unresolved issues of consequence to the formation of landforms on Mars, the one with the greatest implication for possible slope processes is the abundance of H_2O ice in the regolith near the surface. Studies of Martian impact crater morphology have generally taken the presence of craters surrounded by unusually large ejecta-flow deposits in the latitudinal bands along 40°N and 45°S to be evidence of H_2O near the surface (Mouginis-Mark 1979; 1987; Squyres 1979; Barlow 1994). Areas of fretted terrain in the northern hemisphere may present the best case for volatile-controlled surface modification. These regions are composed of isolated mesas with steep valley wall profiles separated by level surfaces and are found between 30°N and 50°N and in isolated locations at equivalent latitudes of the southern hemisphere (Carr 1986). Under current Martian conditions, H_2O ground ice is unstable between 40°N and 40°S and will sublime to the atmosphere from near-surface regolith (Farmer and Doms 1979). The occurrence of fretted terrain only in the areas above equatorial latitudes has prompted several investigators to suggest that ground ice processes may mobilise slope materials in the mid-latitude regions (Carr 1981; 1986; Rossbacher and Judson 1981; Lucchitta 1984).

The most obvious means for destabilising slopes in the fretted terrain is the exposure of

subsurface volatiles contained behind valley walls either suddenly by tectonic activity or the shock of a meteorite impact or more gradually through the undercutting of scarps by deflation. Once exposed to the surface, the volatiles will sublime and destabilise the resulting slope, which may then collapse to form a debris flow or slowly disintegrate to build a debris apron.

TERRAIN SOFTENING

Squyres and Carr (1986) have identified a global-scale degradation of surface relief at latitudes poleward of 30°. The terrain softening is interpreted to represent a pervasive expression of surface debris movement in response to downslope creep caused by interstitial ice. The three landforms most often associated with terrain softening are convex lobate debris aprons (Squyres 1978), lineated valley fill consisting of multiple ridges parallel to valley walls (Squyres 1979) and concentric crater-fill indicated by circular ridges and grooves within craters (Squyres 1979; Squyres and Carr 1986). In each case, the volatile content is inferred from the ridge-and-groove topography taken to indicate the flow of surface material in a given direction (Squyres 1989).

The distinctive morphology of each type of terrain feature associated with icy regolith has been illustrated primarily with Viking orbiter images of moderate resolution. The available images of greater detail supply clues for an alternative to the volatile-related origin of some terrain-softening features (Zimbelman 1987). The northern mid-latitude regions of Mars show evidence of mantling by materials that uniformly buried surface landforms and were subsequently partially or completely exhumed (Williams and Zimbelman 1988; Moore 1990). High spatial resolution images of deposits both within and around various craters exhibit layering (Zimbelman *et al.* 1988). These characteristics support an aeolian alternative for the deposition and removal of the ubiquitous mantling materials. The distinctive morphology of certain terrain-softening features may be explained as surface expressions of multi-layered aeolian deposits subjected to differential weathering and erosion. At equivalent latitudes in the southern hemisphere basin of Hellas Planitia, a widespread aeolian mantle blankets much of the region (Tanaka and Leonard 1994).

MASS WASTING

Within the equatorial canyons, numerous talus chutes form a spur-and-gully morphology entrenched into canyon walls (Lucchitta 1978a). The shapes and spacings of the talus chutes change from irregular crenations dissecting the resistant caprock of canyon walls to parallel chutes uniformly incised into mesas of layered units located within the canyons (Figure 29.12). The distinctive change in erosional styles within the same region may reflect differing mechanical properties of materials composing wall rocks and layered units. Mass-wasting processes causing lateral slope retreat along escarpments may explain the fretted terrain landscapes in the northern hemisphere mid-latitudes and similar areas of the southern hemisphere highlands (Squyres 1979).

DEBRIS AVALANCHES

At the larger scale, gravity driven processes on Mars have resulted in the creation of colossal landslide debris avalanches triggered by catastrophic slope failure. The most conspicuous avalanche deposits occur in the deep, broad-floored Valles Marineris canyon system between 50°W and 90°W (Figure 29.13A). In this region several dozen debris avalanche deposits ranging in size between 40 and 7000 km^2 have been discovered (Lucchitta 1978b; 1979; 1987; McEwen 1989).

The landslides in Valles Marineris were triggered along canyon walls with heights of 2–7 km and slopes of about 30°. The uppermost sections of the canyon walls are interpreted to be resistant sills of lava, while the underlying materials may be composed of regolith (Lucchitta 1979). The proximal areas of many debris avalanches display giant backward-rotated slide blocks of the resistant units underlying the plateau surface. Hummocky topography often appears downflow from the slide blocks and probably represents coherent megablocks transported far from the collapse

Figure 29.12 *Mass wasting of two different lithologies in the Candor Chasma region (6°S, 71°W) produces irregular crenations (A) along canyon walls and parallel chutes (B) incised into layered deposits with the canyon. [Viking Orbiter mosaic]*

amphitheatre. The distal reaches of most Martian landslides are characterised by longitudinal ridges and grooves radiating outward tens of kilometres from the avalanche source (Figure 29.13B). In several instances flow levees have formed along the lateral margins of an avalanche, but are usually absent along the distal margin.

One possible mechanism for the emplacement of debris avalanches in Valles Marineris has been suggested to be high-velocity mudflows resulting from the sudden outbreak of liquid water from an aquifer held behind an ice lens rising high in the canyon wall (Lucchitta 1979; 1987). The predominance of longitudinal ridge and groove terrain, the extremely low apparent coefficient of friction implied by long avalanche travel distances and the estimated high velocities of emplacement led Lucchitta to the conclusion that Martian avalanches must have been lubricated by water. Recent work on terrestrial volcanic debris avalanches challenges this interpretation.

In a study of the major volcanic debris avalanches in the central Andes, Francis and Wells (1988) discovered a suite of components

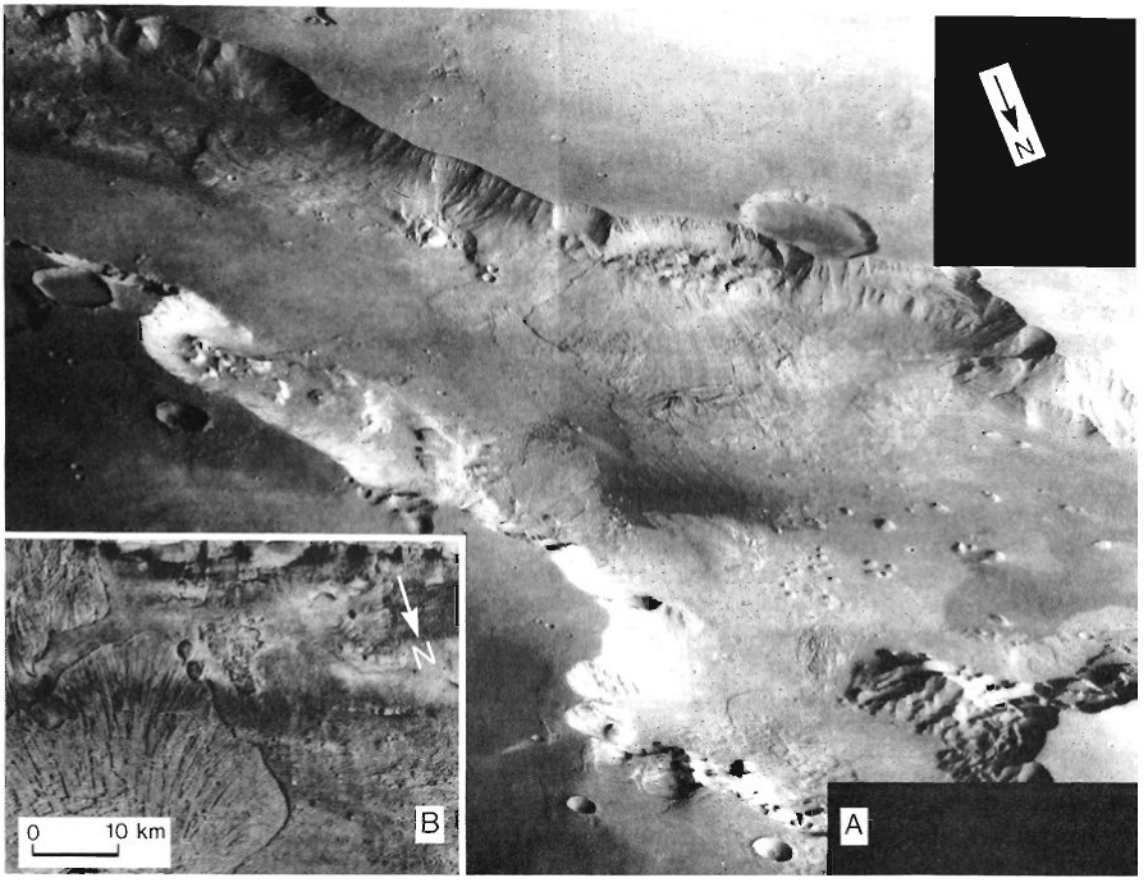

Figure 29.13 *The deposits of giant landslides are found on the floor of Valles Marineris. (A) An oblique view across Ganges Chasma (9°S, 45°W) shows landslides with coherent slide blocks alongside collapse amphitheatres and debris streams radiating far from the avalanche source areas. (B) A detailed view illustrates the longitudinal ridges and grooves in the distal portion of a debris avalanche deposit in Coprates Chasma (11°S, 67°W). [(A) Viking Orbiter mosaic; (B) VO #080A01]*

(rotated slide blocks, hummocky topography, longitudinal ridges and grooves, and marginal levees) reflecting elements of Martian landslides. While Lucchitta (1979; 1987) presumes that the occurrence of longitudinal ridge and groove terrain is rare for terrestrial avalanches, the deposits emplaced from the Lastarria, Llullaillaco, Aucanquilcha, San Pedro and Irruputunca volcanoes on the Andean Altiplano are dominated by such radiating linear features (Naranjo and Francis 1987; Francis and Wells 1988; de Silva and Francis 1991). The well-studied Socompa volcano debris avalanche deposit in northeastern Chile possesses each of the Martian landslide components (Francis and Self 1987; Francis 1993), yet lacks any evidence for water-mobilised emplacement in the form of debris-flow–mudflow transitions, runoff channels or ice escape structures. The Andean landslide deposits with ridge and groove terrain appear to have been formed as dry debris avalanches deposited by enormous sturzstroms (Hsü 1975; Melosh 1979; Francis and Wells 1988; Campbell 1989). Calculations of the yield strength of materials involved in Martian landslides are similar to values obtained for dry debris avalanches on Earth (McEwan 1989). From these lines of evidence, it may be concluded that Martian landslides flowed across the surface in a similar manner without the aid of a lubricating fluid.

Climatic change on Mars

The most ancient terrains on Mars show ample evidence of water flowing across the surface during the first several hundred million years of the planet's geological history (Pieri 1980; Baker 1982). More controversial interpretations of the Martian landscape have offered clues for the existence of ancient oceans (Baker *et al.* 1991), lacustrine deposits (Parker *et al.* 1989; Scott *et al.* 1992; Williams and Zimbelman 1994) and glacial features (Lucchitta 1982; Kargel and Strom 1992), though such contentions remain highly speculative. During the present climatic epoch and probably for the past 3 billion or more years, liquid water has not existed on the Martian surface in equilibrium with the atmosphere. Despite the absence of liquid water and an Earth-like hydrological cycle, some regions of Martian landforms indicate a response to climatic fluctuations occurring on a timescale between 10 000 and 1 million years.

MARTIAN MILANKOVITCH CYCLES

On Earth, slight changes in the angle of the spin axis to the orbital plane (obliquity), the axial tilt direction (precession) which controls the seasonal timing of the closest approach to the Sun, and the shape of the orbit around the Sun (eccentricity) produce cyclical differences in the intensity of incoming radiation (Table 29.2). Mars also displays cyclical variations in its orbital geometry (Figure 29.14). The changes are much greater for Mars because its obliquity cycle encompasses a much greater range of values. The most important characteristic of the Martian Milankovitch cycles is their combined effect upon the amplitude of insolation change. Terrestrial ice ages and deglaciations appear to be determined by high-latitude insolation variations of about 8% (Kutzbach 1987). Martian changes of high-latitude insolation approach 50% during a million-year cycle (Murray *et al.* 1973), and obliquity forced insolation changes may have been even greater over the past 10 million years (Bills 1990).

EVIDENCE FOR CHANGING CIRCULATION PATTERNS

The polar regions contain layered deposits almost unblemished by impact craters, which suggests a surface age of only a few million years. Each layer extends uniformly over a vast area and is approximately 30 m thick. High- and low-albedo units alternate to form a sequence of layered deposits exposed along spiral troughs radiating outward from the poles (Figure 29.15). At the highest latitudes of the northern hemisphere, a perennial H_2O ice cap rests upon the polar layered deposits (Kieffer *et al.* 1976), whereas a perennial CO_2 frost cap covers the South Pole (Kieffer 1979). The albedo of the north polar ice cap is only about 0.4, an indication of substantial aeolian sediment mixed with the ice (Kieffer *et al.* 1977).

A model proposed to account for deposition of polar layered deposits is regulated by the climatic change created by Milankovitch cycles (Toon *et al.* 1980). At times of low obliquity (12–20°), atmospheric CO_2 condenses in the polar regions and leads to a decrease in atmospheric pressure to about 1 mb, thus halting the movement of windblown sediments. During periods of low obliquity, largely sediment-free H_2O ice and CO_2 ice are deposited at the poles. When Martian obliquity reaches high values (30–38°), CO_2 ice sublimes from the poles and regolith to raise atmospheric pressure to perhaps 30 mb (Toon *et al.* 1980; François *et al.* 1990). The increased temperature gradient near

Table 29.2 *Milankovitch cycles for Mars and Earth (years)*

	Mars	Earth
Obliquity	1.2×10^5 and 1.3×10^6	9.5×10^4
Eccentricity	9.5×10^4 and 2.0×10^6	4.1×10^4
Precession	7.2×10^4 and 1.7×10^5	2.3×10^4 and 1.9×10^4

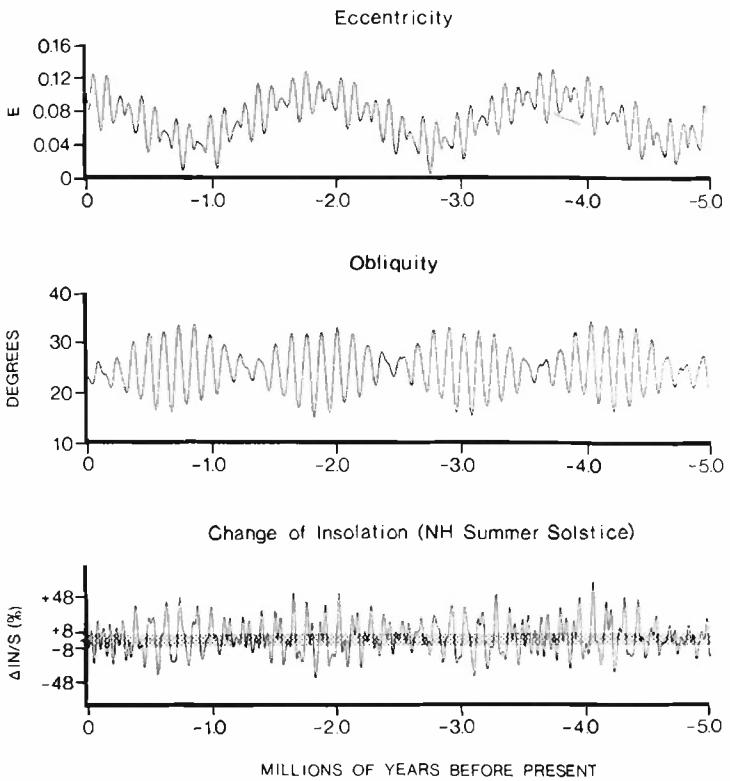

Figure 29.14 *Cyclical changes of Martian orbital eccentricity and obliquity cause periodic fluctuations in the amount of incident radiation. The shaded portion of the northern hemisphere insolation curve represents the range of variation in the Earth's insolation during the past 5 million years*

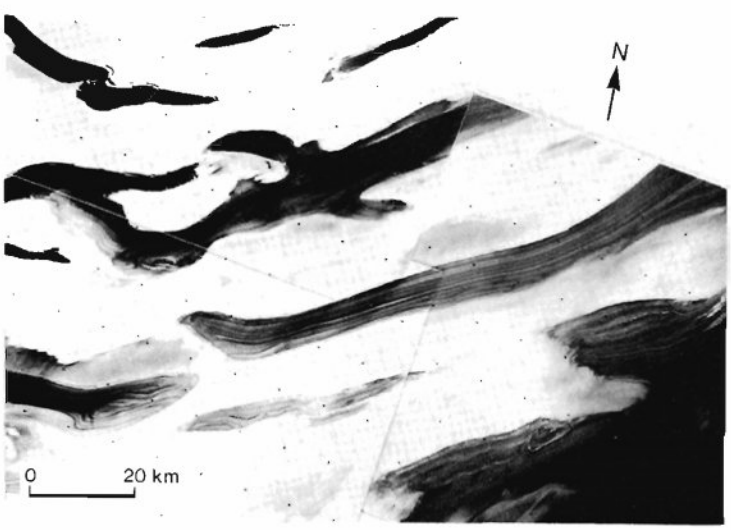

Figure 29.15 *Alternating bright and dark units compose the terrain of layered deposits in the north polar region (82°N, 269°W). [VO #0065B67-69]*

the polar caps and higher atmospheric pressure promote frequent global dust storms and saltation events during summer in both hemispheres. During periods of high obliquity, condensates of dusty ice accumulate on the winter pole. The colour and albedo characteristics of polar layered deposits are consistent with a mixture of dusty ice and saltated sediment (Herkenhoff and Murray 1990b). Following sublimation, a dark layer of aeolian sediment will insolate the underlying ice to produce alternating bright and dark bands deposited under high- and low-obliquity conditions. A 120 000-year cycle controls layer deposition, according to this hypothesis (Toon *et al.* 1980).

Layered deposits without volatiles are found at equatorial latitudes. In the region of Amazonis Planitia (7°N, 141°W), the deposits are 3.5 km in thickness with individual layers of about 100 m. Two sets of yardangs with directions nearly perpendicular to each other have formed upon the layered deposits (Figure 29.16). The older, northward-trending yardangs are partially buried by the uppermost layer. Deflation by easterly winds created the younger yardangs and exhumed the older set.

A model to explain the sequence of layer deposition and yardang formation by winds of different directions invokes climatic change governed by the Milankovitch cycles (Zimbelman and Wells 1987). During periods of low obliquity, no aeolian sedimentation occurs, and an indurated horizon may form in the upper portion of the surface layer. At a time of high obliquity (or intermediate obliquity, high eccentricity and perihelion during northern hemisphere summer), cross-equatorial airflow returning to the northern hemisphere etched the set of yardangs aligned north–south (Figure 29.17A). During a phase of intermediate obliquity and low to intermediate eccentricity, convergent circulation along the equator produces easterly winds that transport sediments from the Tharsis Montes region and beyond for deposition in Amazonis Planitia (Figure 29.17B). Possible southern sources for the aeolian mantle burying the north–south yardang set are excluded by the apparent lack of sediments within that region during the preceding interval when yardangs were etched by southerly winds. Following the decline of available sediments from eastern source regions, the uppermost layer was excavated by easterly winds to expose the older yardang set and create a new set of east–west yardangs (Figure 29.17C). Though the Amazonis Planitia layered deposits comprise one of the youngest surfaces on Mars, it is unlikely that the episodic layer deposition and yardang formation represent the consequences of a single obliquity cycle.

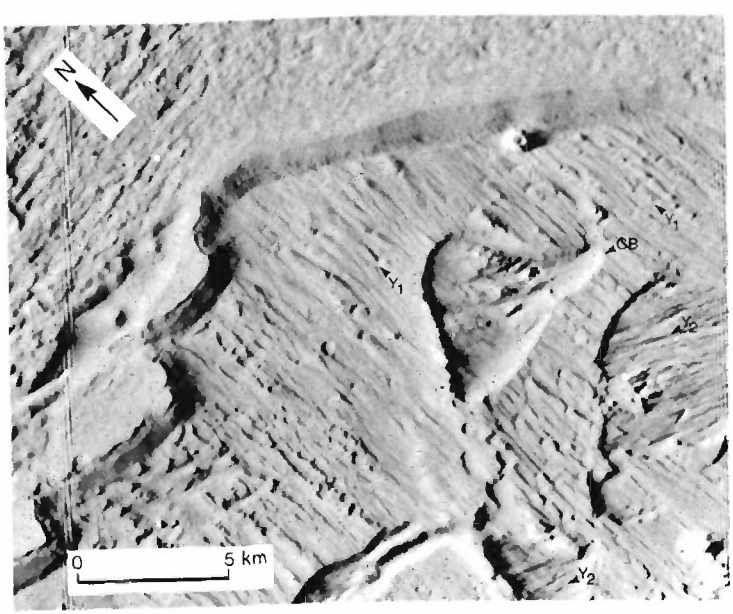

Figure 29.16 *Two sets of yardangs were formed by winds of different directions in the Amazonis Planitia region (7°N, 141°W). The older yardangs (Y_1) were buried by a deposit 100 m in thickness and later exposed by easterly winds that formed the younger yardangs (Y_2) and a cuspate deflation basin (CB). [VO #471S18]*

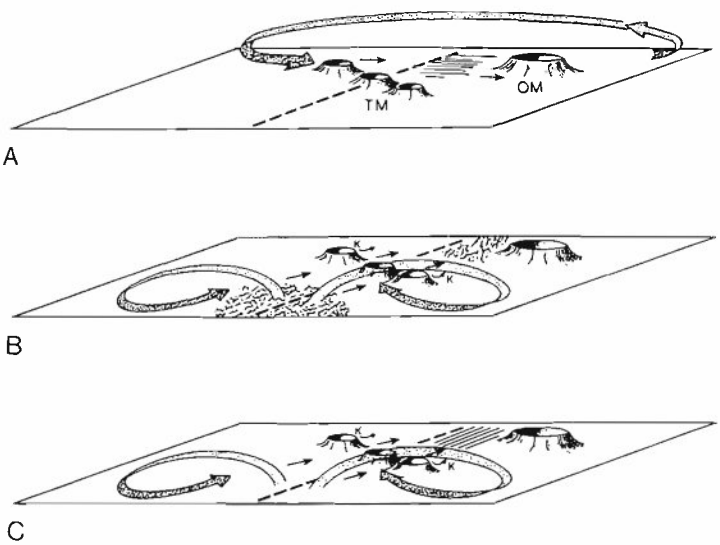

Figure 29.17 *A model to account for episodic layer deposition and yardang formation in the Amazonis Planitia region to the south of Olympus Mons (OM). (A) The older yardang set is eroded by circulation linked to a period of high obliquity (or intermediate obliquity, high eccentricity and northern hemisphere perihelion). (B) During a period of intermediate obliquity, convergent circulation transport sediments from the east of Tharsis Montes (TM) with additional material carried by katabatic winds (K) from the volcanic massif. (C) The younger yardangs form after the eastern source of sediments diminishes*

Arid surface processes on Venus

With a surface temperature hotter than the melting point of lead, Venus offers a near-ultimate case for the action of arid surface processes. While seemingly exotic in many aspects, the forces shaping the Venusian landscape can produce results which are surprisingly terrestrial in their final forms, making Venus more a twin of our own planet than many would expect based upon general physical principles (Table 29.1). Information gained from the Magellan radar mapping mission of the early 1990s established that, like Earth, most of the surface of Venus is geologically young with an age of less than 500 million years (Head 1994; Strom *et al.* 1994). Unlike Earth, however, with its oceanic basins, mobile continental plates and continually recycled crust, Venus experienced a global volcanic flooding event which covered the entire planet with mafic silicate basalts approximately 300 million years ago (Kargel 1994). Physiographically, 65% of the Venusian surface consists of rolling plains, 27% lies in basins below the mean surface datum (the 6051 km planetary radius), and 8% forms highlands with altitudes greater than 2 km (Sharpton and Head 1986). Most of Venus is covered by exposed bedrock with only about one-quarter of the surface overlain by unconsolidated sediments (Greeley 1994).

The abundance of carbon dioxide in the atmosphere, coupled with trace amounts of sulphur dioxide, sulphuric acid and water vapour, produces an extreme greenhouse effect, warming the surface by an additional 227°C (Cattermole 1994). High surface temperatures are held constant because the obliquity of the Venusian rotation axis creates no seasonal changes of insolation between hemispheres (Sagan 1976), and heat retention by the dense atmosphere allows only a 1–3°C difference between day and night-time temperatures (Zolotov and Volkov 1992). Differences in surface temperature and pressure stem solely from changes in altitude and vary from 465°C and 96 bars at the lowest elevations to 374°C and 41 bars at peak elevations in the highlands (Greeley 1994). The high level of atmospheric carbon dioxide is probably buffered by the mineral reaction between calcite and quartz producing wallastonite and carbon dioxide, a reaction favoured by the range of surface temperatures and pressures on Venus (Urey 1952; McGill *et al.* 1983). Chemically reactive gases (CO, CO_2, COS, SO_2, H_2O, H_2S, HCl, HF) in the lower Venusian atmosphere raise the possibility of surface weathering by gas–solid interactions (Florensky *et al.* 1976; Nozette and Lewis 1982; Zolotov and Volkov 1992). Although mixing ratios of corrosive gases in the lower atmosphere are poorly known, chemical

analyses performed using X-ray florescence at three landing sites (Venera 13, 14; Vega 2) suggest an enrichment of sulphur in surface materials as a result of chemical weathering processes (Basilevsky *et al.* 1992). Another sign of weathering is the near-infrared brightness of soil and surface rocks at the Venera 13 landing site, which may be attributable to the formation of ferric oxides in an oxidising environment (Pieters *et al.* 1986).

Altitude-dependent chemical weathering processes may explain an unusual feature detected by the Magellan radar imaging system. At elevations approximately 2.8 km above the mean planetary radius, a sharp boundary occurs between lower regions having low radar reflection coefficients and highland areas with high reflection coefficients (Arvidson *et al.* 1991; 1992; Tyler *et al.* 1991). Contacts between radar-bright and radar-dark surfaces can be traced for hundreds of kilometres with little change in elevation, leading to the conclusion that a global chemical phase change controlled by atmospheric temperature and pressure occurs at a specific altitude above the surface. Such a phase change would alter the dielectric constant of exposed rock surfaces by producing a different kind of weathering crust containing magnetite, haematite, ilmenite or other minerals that remain unstable at lower elevations (Arvidson *et al.* 1991; Zolotov and Volkov 1992). At still higher elevations, surfaces again become radar-dark in areas where highland summit rocks may be coated with pyrite-bearing minerals stable only at the highest elevations on Venus (Arvidson *et al.* 1992). An intriguing consequence of these chemical equilibrium changes is the possibility that metal halides liberated in vapour state in the hot (*c.* 460°C) lowlands of Venus are transported by atmospheric circulation to higher, cooler (*c.* 380°C) elevations, where they precipitate to create a uniform surface layer (Brackett *et al.* 1994). Crystal growth in rock pore spaces by condensing metal halides may mechanically destroy highland rocks and may explain the increased radar roughness characteristics noted for highland terrains.

Despite ample evidence for active chemical weathering processes on Venus, most fine granular material on the surface appears to originate from ejecta blankets deposited during impact crater formation (Garvin 1990) with, perhaps, minor additional contributions from volcanic eruptions of basaltic cinders and ashes (Basilevsky *et al.* 1992). In contrast to Earth and Mars, the sandblasting of surface rocks does not play a significant role in particle formation. Aeolian abrasion of coherent rocks is orders of magnitude less efficient on Venus than on Earth and Mars because low surface wind velocities fail to transmit sufficient kinetic energy to airborne mineral grains (McGill *et al.* 1983). As documented in a series of panoramic views relayed by the Venera 13 lander showing the sequential removal of fine materials from the lander support ring, aeolian transport of sediments by saltation and suspension occurs on Venus (Basilevsky *et al.* 1992). Wind-tunnel experiments under Venusian surface conditions confirm that saltation involving a 0.06 mm grain will take place at a threshold friction speed of 0.17 $m\,s^{-1}$ (Iversen and White 1982; White 1986), which may be extrapolated to a wind velocity of approximately 1 $m\,s^{-1}$ measured at a level 1 m above the surface (Figure 29.7). Saltation path lengths are short and trace low-angle trajectories on Venus, and should create ripple-scale bedforms having higher amplitudes and shorter wavelengths than terrestrial sand ripples (Greeley and Iversen 1985). An unusual characteristic of basaltic materials placed in saltation under the high temperatures and pressures of the Venusian surface is the growth of thin weathering veneers created by debris comminuted from basaltic grains onto impacted rock surfaces (Greeley *et al.* 1987).

In a manner similar to comparable features on Mars, wind-streaks on Venus are closely associated with impact craters, volcanic domes and other topographic barriers that disrupt and accelerate airflow (Figure 29.18). Radar-bright streaks typically extend 10–20 km in the lee of obstructions and represent zones swept free of aeolian sediments (Greeley *et al.* 1992a); thus, the radar-bright streaks of Venus correspond to the visibly dark crater streaks seen on Mars (Figure 29.5). Other wind-streaks are radar-dark and represent the concentration of a surface layer of unconsolidated aeolian sediments at least 10–70 cm deep (Greeley *et al.* 1992a). The global pattern of wind-streak directions can be used to construct a map of prevailing surface winds related to the global Hadley circulation (Schubert 1983; Greeley *et al.*

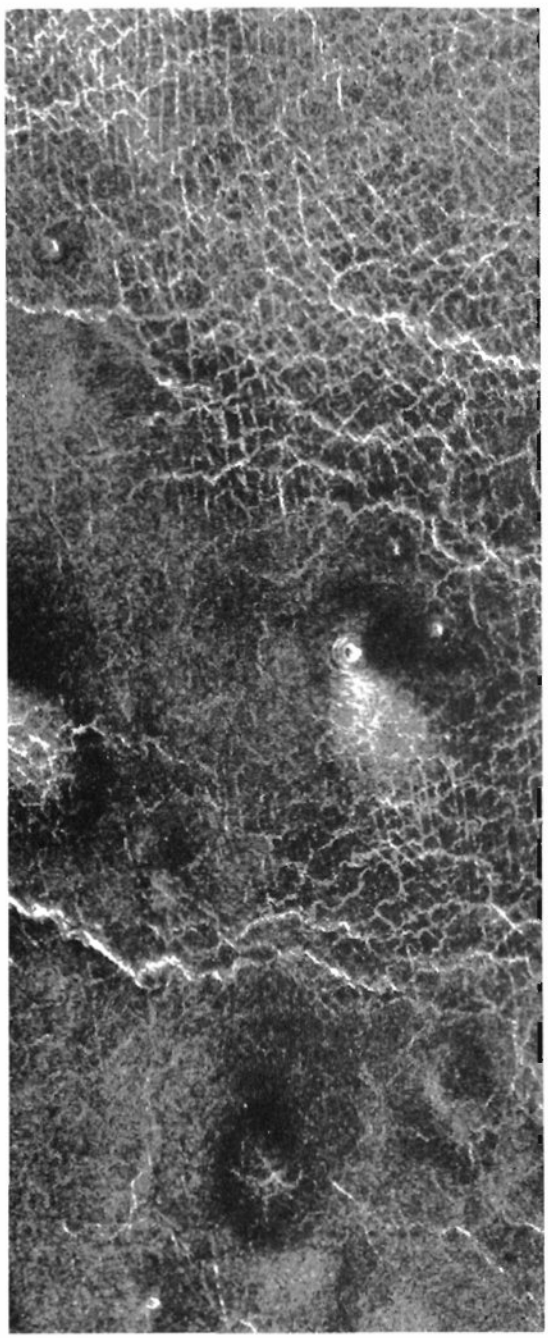

Figure 29.18 *Radar-bright wind-streaks extend in fan-shaped patterns in the lee of small volcanic cones in the Guinevere Planitia region of Venus (22.3°N, 332.1°E). [Magellan F-MIDR #20N334]*

1994). On Venus, the general circulation is symmetrical about the equator and consists of rising limbs of Hadley cells along the equator, poleward winds aloft, downflow over the polar regions and equatorward surface winds. A global map of wind-streak directions beautifully reflects the strongly meridional character of Venusian surface winds (Greeley *et al.* 1994).

Evidence for aeolian deposition on Venus includes landscape features created by both dust- and sand-sized particles. Dark horseshoe-shaped haloes associated with young impact craters are thought to be the consequence of pre-impact shock waves which swept dust from the surface to altitudes greater than 10 km, where the dust clouds interacted with easterly winds of the atmospheric super-rotation (Arvidson *et al.* 1992; Greeley *et al.* 1992a). The parabolic haloes of radar-dark sediments extend hundreds of kilometres to the west of several of the largest and youngest craters in a pattern which suggests aeolian dispersal by easterly winds. Given the low rate of large impact crater formation during the past billion years, the presence of parabolic haloes adjacent to approximately 10% of all large craters leads to the conclusion that dust deposits may persist as distinct units for tens of millions of years on the Venusian surface (Arvidson *et al.* 1992).

Imaging radar systems do not facilitate detection of aeolian bedforms because dry, granular sediments are poor radar reflectors. Despite this inherent difficulty in the use of Magellan radar imagery, two small dunefields have been located on Venus. The Algaonice dunefield (25°N, 340°E) of transverse ridge bedforms covers 1290 km^2 and lies near the radar-bright ejecta deposits of Algaonice Crater (Greeley *et al.* 1992a). The Fortuna–Meshkenet dunefield (67.7°N, 90.5°E) is also situated in a heavily cratered region and contains 17 120 km^2 of transverse dunes. Bedform lengths of the transverse dunes range from 0.5 to 10 km with average widths of 200 m and crest-to-crest spacings of approximately 500 m (Greeley *et al.* 1992a). The apparent scarcity of dunes on Venus may be related to the limited supply of saltable sediments available from crater ejecta blankets. Alternatively, there may remain many undiscovered dunes on Venus which are simply too small to be detected by the Magellan imaging radar system.

Another kind of aeolian deposit may be more ubiquitous than any other discussed in this section. It is possible that the bedded slab-like rocks seen in surface views of the Venera 10, 13 and 14 landing sites are indurated aeolian sediments (Florensky *et al.* 1977; McGill *et al.* 1983). The low bulk density (*c.* 2 $g cm^{-3}$) of rock samples examined at the sites is consistent with the expected properties of an extraterrestrial eolianite (McGill *et al.* 1983).

Although wind erosion is orders of magnitude less effective on Venus than on Earth and Mars, yardang-like features are present in the region of Aphrodite Terra (9°N, 60.5°E) and have been ascribed to the aeolian stripping of a friable ejecta deposit derived from Meade Crater (Greeley *et al.* 1992a). The parallel ridges and grooves attain lengths of 25 km with widths of 0.5 km and are aligned in the same direction as wind-streaks in the region.

Mass-wasting processes are apparent in surface views of the Venusian landscape and from radar imagery of highland regions. At the Venera 9 landing site, the panoramic scene displayed detached rocks and slab-like boulders descending a 20° slope (Florensky *et al.* 1977). Steep slopes in mountainous regions serve as sources for slump blocks and large landslides observed on radar images (Arvidson *et al.* 1991; Malin 1992). Debris avalanche deposits resembling those emplaced by giant terrestrial and Martian landslides occur in the region of Maxwell Montes (Vorder-Bruegge 1994).

Careful inspection of the landforms discovered to date on Venus has yet to reveal any evidence for climatic change. Since Venus does not experience significant cyclical variations in its orbital geometry, a possible mechanism for global climatic change is not readily apparent. It would seem that Venus has suffered a monotonously torrid environment for at least the last several hundred million years.

Future planetary research

After reading this review of the current state of knowledge concerning arid surface processes on Mars and Venus, one may be interested in the prospects for resolving some areas of debate with information returned from future planetary missions. Several missions are planned for the remainder of the century.

The Mars Global Surveyor (MGS) spacecraft is scheduled to provide the initial recovery following the loss of the Mars Observer spacecraft in 1993. Three of the MGS instruments will be of particular importance to investigations of arid surface processes on Mars. The Mars Observer Camera (MOC) will provide global synoptic images of clouds and large regions of the surface at low spatial resolution (7.5 km per pixel) and many very high resolution (1.4 m per pixel) views of selected sites around the planet (Malin *et al.* 1992). The Thermal Emission Spectrometer (TES) will gather emission spectra of the surface and atmosphere in the 6 to 50 μm range at a spatial resolution of 3 km (Christensen *et al.* 1992). The Mars Observer Laser Altimeter (MOLA) will obtain altimetry measurements with 1.5 m vertical resolution over 160 m swaths, which will generate surface elevations and gradients over a global grid of $0.2° \times 0.2°$ cells (Zuber *et al.* 1992). The Mars Global Surveyor is scheduled to be placed into a mapping orbit around Mars in 1998. Images and measurements by the MOC, TES and MOLA will permit new numerical tests to be applied to many of the hypotheses discussed in this chapter regarding surfaces processes, landform development, the existence of volatiles and the climatic history of Mars.

Another NASA spacecraft should arrive on Mars before the MGS mission. Mars Pathfinder is scheduled to place an instrumented lander on the Martian surface in July of 1997. The lander's colour imaging system will have the capability to generate stereoscopic views and to image wind socks at three discrete heights above the Martian surface, providing the first extraterrestrial measurements of boundary layer structure. A small solar-charged, battery-powered, 'rover' vehicle will carry an alpha proton X-ray spectrometer to be placed in direct contact with rocks identified using the lander's colour imaging system (Golombek and Spear 1994). Mars Pathfinder is designed primarily as an engineering test-bed, but important scientific results should be obtained during its mission.

Several other advanced spacecraft missions are currently under study by NASA, the European Space Agency and the space agencies

of Japan and Russia. If funded and launched, most of the missions will make use of miniaturised science and engineering components that reduce the required size and mass of a spacecraft while enhancing the potential scientific return from their data.

The ultimate goal of various spacecraft missions is to prepare the way for human exploration. Only then can some of the issues raised in this review reach a satisfactory resolution. Afterwards we can look forward to the kind of stimulating debate concerning the arid surfaces of Mars and Venus that followed unexpected discoveries during the initial exploration of remote regions of the Earth.

References

Arvidson, R., Guiness, E. and Lee, S. 1979. Differential aeolian redistribution rates on Mars. *Nature*, 278: 533–535.

Arvidson, R.E., Baker, V.R., Elachi, C., Saunders, R.S. and Wood, J.A. 1991. Magellan: initial analysis of Venus surface modification. *Science*, 252: 270–275.

Arvidson, R.E., Greeley, R., Malin, M.C., Saunders, R.S., Izenberg, N., Plaut, J.J., Stofan, E.R. and Shepard, M.K. 1992. Surface modification of Venus inferred from Magellan observations of plains. *Journal of Geophysical Research*, 97: 13303–13317.

Baird, A.K., Toulmin, P., Clark, B.C., Rose, H.J. Jr, Keil, K., Christian, R.P. and Gooding, J.L. 1976. Mineralogic and petrologic implications of Viking geochemical results from Mars: interim report. *Science*, 194: 1288–1293.

Baker, V.R. 1982. *The channels of Mars*. University of Texas Press, Austin.

Baker, V.R., Strom, R.G., Gulick, V.C., Kargel, J.S., Komatsu, G. and Kale, V.S. 1991. Ancient oceans, ice sheets and the hydrological cycle on Mars. *Nature*, 352: 589–594.

Barlow, N.G. 1994. Impact craters as indicators of subsurface H_2O on Mars. *Lunar and Planetary Science Conference*, 25: 59-60 (abstract).

Barnes, J.R. 1990. Transport of dust to high northern latitudes in a Martian polar warming. *Journal of Geophysical Research*, 95: 1381–1400.

Barnes, J.R., Pollack, J.B., Haberle, R.M., Leovy, C.B., Zurek, R.W., Lee, H. and Schaeffer, J. 1993. Mars atmospheric dynamics as simulated by the NASA Ames general circulation model, 2. Transient baroclinic eddies. *Journal of Geophysical Research*, 98: 3125–3148.

Basilevsky, A.T., Nikolayeva, O.V. and Kuzmin, R.O. 1992. Resurfacing. In V.L. Barsukov, A.T. Basilevsky, V.P. Volkov and V.N. Zharkov (eds), *Venus geology, geochemistry, and geophysics*. University of Arizona Press, Tucson: 153–160.

Bills, B.G. 1990. The rigid body obliquity history of Mars. *Journal of Geophysical Research*, 95: 14137–14153.

Bowler, J.M. 1973. Clay dunes: their occurrence, formation and environmental significance. *Earth Science Reviews*, 9: 315–378.

Brackett, R.A., Fegley, B. Jr and Arvidson, R.A. 1994. Vapor transport, weathering, and the highlands of Venus. *Lunar and Planetary Science Conference*, 25: 157–158 (abstract).

Breed, C.S., Grolier, M.J. and McCauley, J.F. 1979. Morphology and distribution of common 'sand' dunes on Mars: comparison with the Earth. *Journal of Geophysical Research*, 84: 8183–8204.

Briggs, G.A., Baum, W.A. and Barnes, J. 1979. Viking orbiter imaging observations of dust in the martian atmosphere. *Journal of Geophysical Research*, 84: 2795–2820.

Burns, R.G. 1994. Schwertmannite on Mars: deposition of this ferric oxyhydroxysulfate mineral in acidic saline meltwaters. *Lunar and Planetary Science Conference*, 25: 203–204 (abstract).

Burns, R.G. and Fisher, D.S. 1990. Iron–sulfur mineralogy of Mars: magmatic evolution and chemical weathering products. *Journal of Geophysical Research*, 95: 14415–14421.

Campbell, C.S. 1989. Self-lubrication for long runout landslides. *Journal of Geology*, 97: 653–665.

Carr, M.H. 1981. *The surface of Mars*. Yale University Press, New Haven, CT.

Carr, M.H. 1986. Mars: a water-rich planet? *Icarus*, 68: 187–216.

Cattermole, P. 1994. *Venus*. Johns Hopkins University Press, Baltimore.

Christensen, P.R. 1986a. Seasonal variability of Martian surface albedos: implications for dust deposition and removal. *Lunar and Planetary Science Conference*, 17: 121–122 (abstract).

Christensen, P.R. 1986b. Regional dust deposits on Mars: physical properties, age, and history. *Journal of Geophysical Research*, 91: 3534–3536.

Christensen, P.R. 1986c. The spatial distribution of rocks on Mars. *Icarus*, 68: 217–238.

Christensen, P.R. 1988. Global albedo variations on Mars: implications for active aeolian transport, deposition, and erosion. *Journal of Geophysical Research*, 93: 7611–7624.

Christensen, P.R., Anderson, D.L., Chase, S.C., Clark, R.N., Kieffer, H.H., Malin, M.C., Pearl, J.C., Carpenter, J., Bandiera, N., Brown, F.G. and Silverman, S. 1992. Thermal Emission

Spectrometer Experiment: Mars Observer Mission. *Journal of Geophysical Research*, 97: 7719–7734.
Clark, B.C. and Van Hart, D.C. 1981. The salts of Mars. *Icarus*, 45: 370–378.
Clark, B.C., Baird, A.K., Rose, H.J. Jr, Toulmin, P., Keil, K., Castro, A.J., Kelliher, W.C., Rowe, C.D. and Evans, P.H. 1976. Inorganic analyses of Martian surface samples at the Viking landing sites. *Science*, 194: 1283–1288.
de Silva, S.L. and Francis, P.W. 1991. *Volcanoes of the central Andes*. Springer-Verlag, New York.
Donahue, T.M. 1995. Evolution of water reservoirs on Mars from D/H ratios in the atmosphere and crust. *Nature*, 374: 432–434.
Edgett, K.S. and Blumberg, D.G. 1994. Star and linear dunes on Mars. *Icarus*, 112: 448–464.
Edgett, K.S. and Christensen, P.R. 1991. The particle size of martian aeolian dunes. *Journal of Geophysical Research*, 96: 22765–22776.
Farmer, C.B. and Doms, P.E. 1979. Global seasonal variation of water vapor on Mars and the implications for permafrost. *Journal of Geophysical Research*, 84: 2881–2888.
Florensky, C.P., Ronca, L.B, Basilevsky, A.T., Burba, G.A., Nikolaeva, O.V., Pronin, A.A., Trakhtman, A.M., Volkov, V.P. and Zazetsky, V.V. 1976. The surface of Venus as revealed by Soviet Venera 9 and 10. *Bulletin of the Geological Society of America*, 88: 1537–1545.
Francis, P.W. 1993. *Volcanoes: a planetary perspective*. Clarendon Press, Oxford.
Francis, P.W. and Self, S. 1987. Collapsing volcanoes. *Scientific American*, 256: 90–97.
Francis, P.W. and Wells, G.L. 1988. Landsat Thematic Mapper observations of debris avalanche deposits in the Central Andes. *Bulletin of Volcanology*, 50: 601–621.
François, L.M., Walker, J.C.G. and Kuhn, W.R. 1990. A numerical simulation of climatic changes during the obliquity cycle on Mars. *Journal of Geophysical Research*, 95: 14761–14778.
Garvin, J.B. 1990. The global budget of impact-derived sediment on Venus. *Earth, Moon, Planets*, 50/51: 175–190.
Golombek, M.P. and Spear, A.J. 1994. Mars Pathfinder science investigations and objectives. *Proceedings of the Congress of the International Astronomical Federation*, 45: 1 (abstract).
Goudie, A.S. and Wells, G.L. 1995. The nature, distribution and formation of pans in arid zones. *Earth Science Reviews*, 38: 1–69.
Grant, J.A. and Schultz, P.H. 1987. Possible tornado-like tracks on Mars. *Science*, 237: 883–885.
Greeley, R. 1979. Silt–clay aggregates on Mars. *Journal of Geophysical Research*, 84: 6248–6254.
Greeley, R. 1994. *Planetary landscapes*. Chapman & Hall, London.
Greeley, R. and Iversen, J.D. 1985. *Wind as a geological process on Earth, Mars, Venus and Titan*. Cambridge University Press, Cambridge.
Greeley, R., Iversen, J.D., Pollack, J.B., Udovich, N. and White, B. 1974. Wind tunnel simulations of light and dark streaks on Mars. *Science*, 183: 847–849.
Greeley, R., Williams, S., White, B.R., Pollack, J., Marshall, J. and Krinsley, D. 1984. *Abrasion by aeolian particles: Earth and Mars*. NASA Contractor Report 3788. Washington, DC.
Greeley, R., Marshall, J.R. and Pollack, J.B. 1987. Physical and chemical modification of the surface of Venus by windblown particles. *Nature*, 327: 313–315.
Greeley, R., Arvidson, R.E., Elachi, C., Geringer, M.A., Plaut, J.J., Saunders, R.S., Schubert, G., Stofan, E.R., Thouvenot, E.J.P., Wall, S.D. and Weitz, C.M. 1992a. Aeolian features on Venus: Preliminary Magellan results. *Journal of Geophysical Research*, 97: 13319–13345.
Greeley, R., Lancaster, N., Lee, S. and Thomas, P. 1992b. Martian aeolian processes, sediments, and features. In H.H. Kieffer, B.M. Jakosky, C.W. Snyder and M.S. Matthews (eds), *Mars*. University of Arizona Press, Tucson: 730–766.
Greeley, R., Skypeck, A. and Pollack, J.B. 1993. Martian aeolian features and deposits: comparisons with general circulation model results. *Journal of Geophysical Research*, 98: 3183–3196.
Greeley, R., Schubert, G., Limonadi, D., Bender, K.C., Newman, W.I., Thomas, P.E., Weitz, C.M. and Wall, S.D. 1994. Wind streaks on Venus: clues to atmospheric circulation. *Science*, 263: 358–361.
Griffith, L.L. and Arvidson, R.E. 1994. Mars — It's what's inside that counts. *Lunar and Planetary Science Conference*, 25: 481–482 (abstract).
Guiness, E.A., Leff, C.E. and Arvidson, R.E. 1982. Two years of surface changes seen at the Viking landing sites. *Journal of Geophysical Research*, 87: 10051–100058.
Haberle, R.M. 1986a. The climate of Mars. *Scientific American*, 254 (5): 54–62.
Haberle, R.M. 1986b. Interannual variability of global dust storms on Mars. *Science*, 234: 459–461.
Haberle, R.M., Pollack, J.B., Barnes, J.R., Zurek, R.W., Leovy, C.B., Murphy, J.R., Lee, H. and Schaeffer, J. 1993. Mars atmospheric dynamics as simulated by the NASA Ames general circulation model, 1. The zonal-mean circulation. *Journal of Geophysical Research*, 98: 3093–3123.
Harmon, J.K., Campbell, D.B. and Ostro, S.J. 1982. Dual-polarization radar observations of Mars: Tharsis and environs. *Icarus*, 52: 171–187.
Hartmann, W.K. 1972. *Moons and planets*. Bogden & Quidly, Tarrytown, NY.

Head, J.W. III. 1994. Venus after the flood. *Nature*, 372: 729–730.

Herkenhoff, K.E. and Murray, B.C. 1990a. High-resolution topography and albedo of the south polar layered deposits on Mars. *Journal of Geophysical Research*, 95: 14511–14529.

Herkenhoff, K.E. and Murray, B.C. 1990b. Color and albedo of the south polar layered deposits on Mars. *Journal of Geophysical Research*, 95: 1343–1358.

Hess, S.L., Henry, R.M., Leovy, C.B., Ryan, J.A. and Tillman, J.E. 1977. Meteorological results from the surface of Mars: Viking 1 and 2. *Journal of Geophysical Research*, 82: 4559–4574.

Howard, A.D. 1980. *Effect of wind on scarp evolution on the Martian poles*. NASA Technical Memo, TM 82385: 333–335.

Hsü, K.J. 1975. Catastrophic debris streams (sturzstroms) generated by rockfalls. *Bulletin of the Geological Society of America*, 86: 129–140.

Huguenin, R.L. 1976. Mars: chemical weathering as a massive volatile sink. *Icarus*, 28: 203–212.

Huguenin, R.L. 1982. Chemical weathering and the Viking biology experiments on Mars. *Journal of Geophysical Research*, 87: 10069–10082.

Hunt, G.E. and James, P.B. 1979. Martian extratropical cyclones. *Nature*, 278: 531–532.

Iversen, J.D. and White, B.R. 1982. Saltation threshold on Earth, Mars and Venus. *Sedimentology*, 29: 111–119.

Jakosky, B.M. and Christensen, P.R. 1986. Global duricrust on Mars: analysis of remote-sensing data. *Journal of Geophysical Research*, 91: 3547–3559.

Kahn, R.A., Martin, T.Z. and Zurek, R.W. 1992. The Martian dust cycle. In H.H. Kieffer, B.M. Jakosky, C.W. Snyder and M.S. Matthews (eds), *Mars*. University of Arizona Press, Tucson: 1017–1053.

Kargel, J.S. 1994. An alluvial depositional analog for some volcanic plains on Venus. *Lunar and Planetary Science Conference*, 25: 667–668 (abstract).

Kargel, J.S. and Strom, R.G. 1992. Ancient glaciation on Mars. *Geology*, 20: 3–7.

Kieffer, H.H. 1979. Mars south polar spring and summer temperatures: a residual CO_2 frost. *Journal of Geophysical Research*, 84: 8263–8288.

Kieffer, H.H., Chase, S.C., Miner, E.D., Munch, G. and Neugebauer, G. 1973. Preliminary report on infrared radiometric measurements from the Mariner 9 spacecraft. *Journal of Geophysical Research*, 78: 4291–4312.

Kieffer, H.H., Chase, S.C., Martin, T.Z., Miner, E.D. and Palluconi, F.D. 1976. Martian north pole summer temperatures: Dirty water ice. *Science*, 194: 1341–1344.

Kieffer, H.H., Martin, T.Z., Peterfreund, A.R., Jakosky, B.M., Miner, E.D. and Palluconi, F.D. 1977. Thermal and albedo mapping of Mars during the Viking primary mission. *Journal of Geophysical Research*, 82: 4249–4291.

Kutzbach, J.E. 1987. Model simulations of the climatic patterns during the deglaciation of North America. In W.F. Ruddiman and H.E. Wright, Jr (eds), *North American and adjacent oceans during the last deglaciation*. The geology of North America, Vol. K-3. Geological Society of America, Boulder, CO: 425–446.

Lancaster, N. and Greeley, R. 1987. Mars: morphology of southern hemisphere intracrater dunefields. *Reports of Planetary Geology and Geophysics Program — 1986*. NASA Technical Memo, TM 89810: 264–265.

Lancaster, N. and Greeley, R. 1990. Sediment volume in the north polar sand seas of Mars. *Journal of Geophysical Research*, 95: 10921–10927.

Lee, S.W. and Thomas, P.C. 1995. Longitudinal dunes on Mars: relation to current wind regimes. *Journal of Geophysical Research*, 100: 5381–5395.

Lee, S.W., Thomas, P.C. and Veverka, J. 1982. Wind streaks in Tharsis and Elysium: implications for sediment transport by slope winds. *Journal of Geophysical Research*, 87: 10025–10041.

Leovy, C.B. 1979. Martian meteorology. *Annual Review of Astronomy and Astrophysics*, 17: 387–413.

Leovy, C.B. and Zurek, R.W. 1979. Thermal tides and martian dust storms: direct evidence for coupling. *Journal of Geophysical Research*, 84: 2956–2968.

Lucchitta, B.K. 1978a. Morphology of chasma walls, Mars. *Journal of Research of the US Geological Survey*, 6: 651–662.

Lucchitta, B.K. 1978b. A large landslide on Mars. *Bulletin of the Geological Society of America*, 89: 1601–1609.

Lucchitta, B.K. 1979. Landslides in Valles Marineris, Mars. *Journal of Geophysical Research*, 84: 8097–8113.

Lucchitta, B.K. 1982. Ice sculpture in the Martian outflow channels. *Journal of Geophysical Research*, 87: 9951–9973.

Lucchitta, B.K. 1984. Ice and debris in the fretted terrain, Mars. *Journal of Geophysical Research*, 89B: 409–414.

Lucchitta, B.K. 1987. Valles Marineris: wet debris flows and ground ice. *Icarus*, 72: 411–429.

Magalhaes, J.A. 1987. The martian Hadley circulation: Comparison of 'viscous' model predictions to observations. *Icarus*, 70: 442–468.

Magalhaes, J. and Gierasch, P. 1982. A model of martian slope winds: implications for eolian transport. *Journal of Geophysical Research*, 87: 9975–9984.

Mainguet, M. and Chemin, H.-C. 1985. Sand seas of the Sahara and Sahel: an explanation of their

thickness and sand dune type by the sand budget principle. In M.E. Brookfield and T.S. Ahlbrandt (eds), *Eolian sediments and processes*. Elsevier, Amsterdam: 343–352.

Malin, M.C. 1974. Salt weathering on Mars. *Journal of Geophysical Research*, 79: 3888–3894.

Malin, M.C. 1992. Mass movements on Venus: preliminary results from Magellan cycle 1 observations. *Journal of Geophysical Research*, 97: 16337–16353.

Malin, M.C., Danielson, G.E., Ingersoll, A.P., Masursky, H., Veverka, J., Ravine, M.A. and Soulanille, T.A. 1992. Mars Observer Camera. *Journal of Geophysical Research*, 97: 7699–7718.

Mass, C. and Sagan, C. 1976. A numerical circulation model with topography for the martian southern hemisphere. *Journal of Atmospheric Sciences*, 33: 1418–1430.

McCord, T.B. and Westphal, J.A. 1971. Mars: narrow-band photometry, from 0.3 to 2.5 microns, of surface regions during the 1969 apparition. *Astrophysical Journal*, 168: 141–153.

McEwen, A.S. 1989. Mobility of large rock avalanches: evidence from Valles Marineris, Mars. *Geology*, 17: 1111–1114.

McGill, G.E., Warner, J.L., Malin, M.C., Arvidson, R.E., Eliason, E., Nozette, S. and Reasenberg, R.D. 1983. Topography, surface properties, and tectonic evolution. In D.M. Hunten, L. Colin, T.M. Donahue and V.I. Moroz (eds), *Venus*. University of Arizona Press, Tucson: 69–130.

McKee, E.D. 1966. Structures of dunes at White Sands National Monument, New Mexico. *Sedimentology*, 7: 1–69.

Melosh, H.J. 1979. Acoustic fluidization: a new geologic process? *Journal of Geophysical Research*, 84: 7513–7520.

Moore, H.J. and Jakosky, B.M. 1989. Viking landing sites, remote sensing observations, and physical properties of martian surface materials. *Icarus*, 81: 164–184.

Moore, H.J., Hutton, R.E., Clow, G.D. and Spitzer, C.R. 1987. *Physical properties of the surface materials at the Viking landing sites on Mars*. US Geological Survey, Professional Paper, 1389.

Moore, J.M. 1990. Nature of the mantling deposit in the heavily cratered terrain of northeastern Arabia, Mars. *Journal of Geophysical Research*, 95: 14279–14289.

Moore, J.M. and Edgett, K.S. 1993. Hellas Planitia, Mars: site of net dust erosion and implications for the nature of basin floor deposits. *Geophysical Research Letters*, 20: 1599–1602.

Mouginis-Mark, P. 1979. Martian fluidized crater morphology: variations with crater size, latitude, altitude, and target material. *Journal of Geophysical Research*, 84: 8011–8022.

Mouginis-Mark, P.J. 1987. Water or ice in the martian regolith?: clues from rampart craters seen at very high resolution. *Icarus*, 71: 268–286.

Murray, B.C., Ward, W.R. and Yeung, S.C. 1973. Periodic insolation variations on Mars. *Science*, 180: 638–640.

Mutch, T.A. and Jones, K.L. 1978. *The martian landscape*. NASA Publication 425.

Naranjo, J.A. and Francis, P. 1987. High velocity debris avalanche at Lastarria volcano in the north Chilean Andes. *Bulletin of Volcanology*, 49: 509–514.

Nozette, S. and Lewis, J.S. 1982. Venus: chemical weathering of igneous rocks and buffering of atmospheric composition. *Science*, 216: 181–183.

Parker, T.J., Saunders, R.S. and Schneeberger, D.M. 1989. Transitional morphology in west Deuteronilus Mensae, Mars: implications for modification of the lowland/upland boundary. *Icarus*, 82: 111–145.

Peterfreund, A.R. 1985. Local dust storms and global opacity on Mars as detected by the Viking IRTM. In S. Lee (ed.), *Workshop on dust on Mars*. LPI Technical Report 85-02. Lunar and Planetary Institute, Houston: 10–14.

Pieri, D.C. 1980. Martian valleys: Morphology, distribution, age, and origin. *Science*, 210: 895–897.

Pieters, C.M., Head, J.W., Patterson, W., Pratt, S., Garvin, J., Barsukov, V.L., Basilevsky, A.T., Khodakovsky, I.L., Selivanov, A.S., Panfilov, A.S., Gektin, Yu.M. and Narayeva, Y.M. 1986. The color of the surface of Venus. *Science*, 234: 1379–1383.

Plaut, J.J., Kahn, R., Guinness, E.A. and Arvidson, R.E. 1988. Accumulation of sedimentary debris in the south polar region of Mars and implication for climate history. *Icarus*, 75: 357–377.

Pleskot, L.K. and Miner, E.D. 1981. Time variability of martian bolometric albedo. *Icarus*, 45: 427–441.

Pollock, J.B., Leovy, C.B., Greiman, P.W. and Mintz, Y. 1981. A martian general circulation experiment with large topography. *Journal of Atmospheric Sciences*, 38: 3–29.

Robertson, D.F. 1987. U.S. Mars Observer seeks global picture. *Astronomy*, 15 (11): 33–37.

Rossbacher, L.A. and Judson, S. 1981. Ground ice on Mars: inventory, distribution and resulting landforms. *Icarus*, 45: 39–59.

Ryan, J.A. and Henry, R.M. 1979. Mars atmospheric phenomena during major dust storms, as measured at surface. *Journal of Geophysical Research*, 84: 2821–2829.

Sagan, C. 1976. Erosion and the rocks of Venus. *Nature*, 261: 31.

Sagan, C., Pieri, D. and Fox, P. 1977. Particle

motion on Mars inferred from the Viking lander cameras. *Journal of Geophysical Research*, 82: 4430–4438.

Saunders, R.S. and Blewett, D.T. 1987. Mars north polar dunes: possible formation from low-density sediment aggregates. *Astonomicheskii Vestnik*, 21: 181–188.

Schubert, G. 1983. General circulation and the dynamical state of the Venus atmosphere. In D.M. Hunten, L. Colin, T.M. Donahue and V.I. Moroz (eds), *Venus*. University of Arizona Press, Tucson: 681–765.

Scott, D.H. and Tanaka, K.L. 1982. Ignimbrites of Amazonis Planitia region of Mars. *Journal of Geophysical Research*, 87: 1179–1190.

Scott, D.H., Chapman, M.G., Rice, J.W. and Dohm, J.M. 1992. New evidence of lacustrine basins on Mars: Amazonis and Utopia Planitia. *Lunar and Planetary Science Proceedings*, 22: 53–62.

Sharp, R.P. and Malin, M.C. 1984. Surface geology from Viking landers on Mars: a second look. *Bulletin of the Geological Society of America*, 95: 1398–1412.

Sharpton, V.L. and Head, J.W. III 1986. A comparison for the regional slope characteristics of Venus and Earth: implications for geologic processes on Venus. *Journal of Geophysical Research*, 91: 7545–7554.

Squyres, S.W. 1978. Martian fretted terrain: flow of erosional debris. *Icarus*, 34: 600–613.

Squyres, S.W. 1979. The distribution of lobate debris aprons and similar flows on Mars. *Journal of Geophysical Research*, 84: 8087–8096.

Squyres, S.W. 1984. The history of water on Mars. *Annual Review of Earth and Planetary Sciences*, 12: 83–106.

Squyres, S.W. 1989. Urey Prize lecture: water on Mars. *Icarus*, 79: 229–288.

Squyres, S.W. and Carr, M.H. 1986. Geomorphic evidence for the distribution of ground ice on Mars. *Science*, 231: 249–252.

Stephens, S.K., Stevenson, D.J., Keyser, L.F. and Rossman, G.R. 1994. Carbonate formation on Mars: Implications of recent experiments. *Lunar and Planetary Science Conference*, 25: 1343–1344 (abstract).

Strom, R.G., Schaber, G.G. and Dawson, D.D. 1994. The global resurfacing history of Venus. *Lunar and Planetary Science Conference*, 25: 1353–1354 (abstract).

Tanaka, K.L. and Leonard, G.J. 1994. Eolian history of the Hellas region of Mars. *Lunar and Planetary Science Conference*, 25: 1379–1380 (abstract).

Thomas, P. 1982. Present wind velocity on Mars: relation to large latitudinally zoned sediment deposits. *Journal of Geophysical Research*, 87: 9999–10008.

Thomas, P. and Gierasch, P.J. 1985. Dust devils on Mars. *Science*, 231: 175–177.

Thomas, P. and Gierasch, P.J. 1995. Polar margin dunes and winds on Mars. *Journal of Geophysical Research*, 100: 5397–5406.

Thomas, P. and Veverka, J. 1979. Seasonal and secular variations of wind streaks on Mars: an analysis of Mariner 9 and Viking data. *Journal of Geophysical Research*, 84: 8131–8146.

Thomas, P.C. and Weitz, C. 1989. Sand dune materials and polar layered deposits on Mars. *Icarus*, 81: 185–215.

Toon, O.B., Pollock, J.B., Ward, W., Burns, J.A. and Bilski, K. 1980. The astronomical theory of climatic change on Mars. *Icarus*, 44: 552–607.

Toulmin, P. III, Baird, A.K., Clark, B.C., Keil, K., Rose, H.J. Jr, Christian, R.P., Evans, P.H. and Kelliher, W.C. 1977. Geochemical and mineralogical interpretation of the Viking inorganic chemical results. *Journal of Geophysical Research*, 82: 4625–4634.

Tsoar, H., Greeley, R. and Peterfreund, A.R. 1979. Mars: the north polar sand sea and related wind patterns. *Journal of Geophysical Research*, 84: 8167–8180.

Tyler, G.L., Ford, P.G., Campbell, D.B., Elachi, C., Pettengill, G.H. and Simpson, R.A. 1991. Magellan: electrical and physical properties of Venus' surface. *Science*, 252: 265–270.

Urey, H.G. 1952. *The planets, their origin and development*. Yale University Press, New Haven.

Veverka, J., Gierasch, P. and Thomas, P. 1981. Wind streaks on Mars: meteorological control of occurrence and mode of formation. *Icarus*, 45: 154–166.

Vorder Bruegge, R.W. 1994. Depositional units in western Maxwell Montes: implications for mountain building processes on Venus. *Lunar and Planetary Science Conference*, 25: 1447–1448 (abstract).

Ward, A.W. 1979. Yardangs on Mars: evidence of recent wind erosion. *Journal of Geophysical Research*, 84: 8147–8166.

Ward, A.W. and Greeley, R. 1984. Evolution of the yardangs at Rogers Lake, California. *Bulletin of the Geological Society of America*, 95: 829–837.

Ward, A.W., Doyle, K.B., Helm, P.J., Weisman, M.K. and Witbeck, N.E. 1985. Global map of eolian features on Mars. *Journal of Geophysical Research*, 90: 2038–2056.

Wells, E.N., Veverka, J. and Thomas, P. 1984. Mars: experimental study of albedo changes caused by dust fallout. *Icarus*, 58: 331–338.

White, B.R. 1986. Particle transport by atmospheric winds on Venus: an experimental wind tunnel

study. In W.G. Nickling (ed.), *Aeolian geomorphology*. The Binghampton Symposium in Geomorphology, International Series, 17. Allen & Unwin, Boston: 57–73.

Williams, S.H. and Greeley, R. 1986. Wind erosion on Mars: impairment by poor saltation cloud development. *Lunar and Planetary Science Conference*, 17: 952–953 (abstract).

Williams, S.H. and Zimbelman, J.R. 1988. Aeolian gradation on Mars: widespread and ancient. *Lunar and Planetary Science Conference*, 19: 1281–1282 (abstract).

Williams, S.H. and Zimbelman, J.R. 1994. 'White Rock': an eroded Martian lacustrine deposit(?). *Geology*, 22: 107–110.

Zimbelman, J.R. 1987. Spatial resolutions and the geologic interpretation of Martian morphology: Implications for subsurface volatiles. *Icarus*, 71: 257–267.

Zimbelman, J.R. and Kieffer, H.H. 1979. Thermal mapping of the northern equatorial and temperate latitudes of Mars. *Journal of Geophysical Research*, 84: 8239–8251.

Zimbelman, J.R. and Wells, G.L. 1987. Geomorphic evidence for climatic change at equatorial latitudes on Mars. *Geological Society of America 100th Annual Meeting*, 19: 905 (abstract).

Zimbelman, J.R., Clifford, S.M. and Williams, S.H. 1988. Terrain softening revisited: photogeological considerations. *Lunar and Planetary Science Conference*, 19: 1321–1322 (abstract).

Zolotov, M.Yu. and Volkov, V.P. 1992. Chemical processes on the planetary surface. In V.L. Barsukov, A.T. Basilevsky, V.P. Volkov and V.N. Zharkov (eds), *Venus geology, geochemistry, and geophysics*. University of Arizona Press, Tucson: 177–199.

Zuber, M.T., Smith, D.E., Solomon, S.C., Muhleman, D.O., Head, J.W., Garvin, J.B., Abshire, J.B. and Bufton, J.L. 1992. The Mars Observer laser altimeter investigation. *Journal of Geophysical Research*, 97: 7781–7797.